

Title

- Human Biophysics as Network Weights: Conditional Generative Models for Dynamic Simulation
- BioMime: Embed Biophysics into Network Weights

Authors

Shihan Ma^{1, 2, †}, Alexander Kenneth Clarke^{1, †}, Kostiantyn Maksymenko³, Samuel Deslauriers-Gauthier^{3, 4}, Xinjun Sheng^{2, 5}, Xiangyang Zhu^{2, 5, *}, and Dario Farina^{1, *}

¹Department of Bioengineering, Imperial College London, London, UK.

²State Key Laboratory of Mechanical System and Vibration, Shanghai Jiao Tong University, Shanghai, China.

³Neurodec, Sophia Antipolis, France.

⁴Inria Center at Université Côte d'Azur, Nice, France.

⁵Meta Robotics Institute, Shanghai Jiao Tong University, Shanghai, China.

Correspondence to d.farina@imperial.ac.uk and mexyzhu@sjtu.edu.cn

[†]These authors contributed equally to this work.

Abstract

Simulations of biophysical systems are fundamental for studying physiological mechanisms and developing human machine interfaces. Whilst advanced numerical methods, such as finite element models, can excel in this task, they are extremely computationally expensive to use when generating a large number of simulations or simulating dynamic events with continuously changing structural parameters. We propose an architecture that uses a conditional generative model to interpolate between the numerical model states, dramatically lowering the modelling time while maintaining a high generation accuracy. As a demonstration of this concept, we present BioMime, a hybrid-structured generative model that enables an accurate, ultra-fast, and arbitrarily high temporal-resolution simulation of a specific biophysical system during dynamic changes. This methodology has wide applications in physiological and clinical research as well as in supporting data augmentation strategies for signal analysis, representing a computationally efficient and highly accurate model for biophysical simulations.

Teaser

Generative models can learn the dynamics of a biophysical system.

Introduction

Biophysical simulations are a cornerstone of modern biomedical research and engineering, allowing initial explorations of experimental hypotheses and fast iterations of designs prior to physical implementation (1, 2). Decades of continuous developments have seen such models go from a few equations, such as in Hodgkin and Huxley's hugely impactful work on spiking neurons (3), to highly complex physics engines and large numerical models with thousands of individual parameters (4). The rapid expansion in the complexity and fidelity of biophysical simulations has played a major role in advancing their corresponding domains (5), and has even generated entirely new avenues of investigation, such as neurophysiological source reconstruction and embodied artificial intelligence (6, 7).

Despite their successes, the increasing complexity of biophysical simulations has come with a corresponding increase in the associated computational burden, which often limits

adoption (5). Computational complexity is particularly problematic when simulating a dynamic event which rapidly changes the modeling conditions, for example the deformation of the volume conductor in a moving forearm (8), or the changes in mechanical response of the tendons in a bending knee (9). The most common way to address these problems is to discretize time, splitting one dynamic simulation into many static simulations. Although the expense to convert a static simulation into a dynamic one is linear with time steps, the prohibitive computational cost of numerical models at each step renders them infeasible in practice to simulate at even low temporal resolutions. This has become a bottleneck for research that requires capturing the time-varying states of the system or requires a multitude of simulations with a vast set of parameters as the inputs (10).

We propose that a better approach to modeling dynamic human systems is to combine transfer learning approaches with conditional generative models (11). Specifically, the generative models are trained with a numerical model's outputs and then used to predict the outputs of the interpolated system states. Such a model could generate samples inexpensively for a variety of static simulations, or continually morph the outputs of an evolving dynamic state. To achieve these aims, we propose BioMime, an AI model that embeds a biophysical system into the weights of a neural network. Compared with the numerical model that takes the role of a teacher, BioMime manifests two main benefits. First, by implicitly learning the generative properties of the teacher simulation, BioMime can quickly expand the data space by interpolating system states. Second, once trained, BioMime is efficient in synthesizing new data promptly, essentially converting the static numerical model into a dynamic one.

BioMime takes the form of a semi-supervised conditional deep latent variable model with an encoder-decoder structure. The encoder takes the numerical outputs and learns a compressed latent representation. The decoder reconstructs a new sample from the latent and the desired simulation parameters (Fig. 1a). This structure allows the model to accurately mimic the internal state of a simulation and then generate samples that replicate a dynamic change in that state. BioMime can also generate realistic samples *ab initio* without using an encoded representation by sampling from a prior. This is achieved by minimizing the Kullback-Leibler (KL) divergence between the sufficient statistics extracted from the latent representation and a gaussian prior (12).

With the above architectures, we demonstrated that training BioMime adversarially using a conditional discriminator (13, 14) contributes to the accurately synthesized outputs that are highly consistent with the numerical ground truths. We further proved that the high accuracy is preserved while interpolating the system states and only begins to decrease when the extrapolated states are largely deviated from the original data space. BioMime is two orders of magnitude faster than the state-of-the-art numerical model when generating the same amount of data. This allows it to quickly construct a dynamic simulation with high temporal resolution by continuously changing the input parameters. We finally showed an example using BioMime to synthesize the changing electrical potentials during dynamic contractions of a human forearm, which matches the biomechanical movements of a musculoskeletal model.

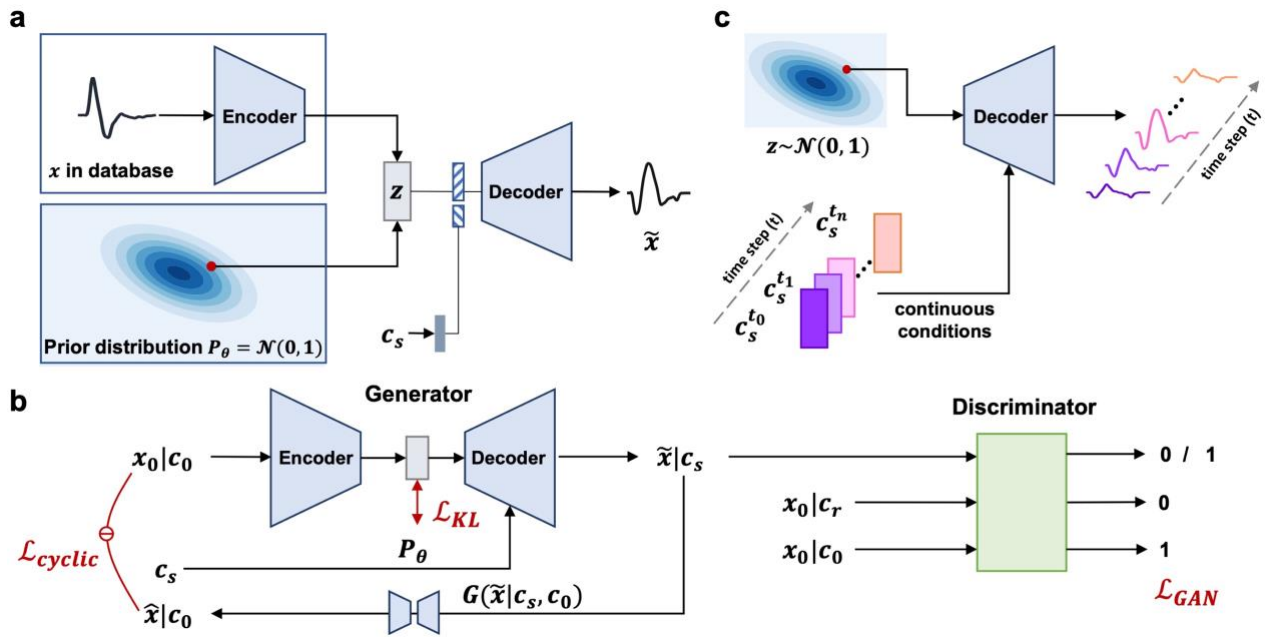


Fig. 1. Deep latent variable model, BioMime. **a**, The generative architecture of BioMime model. BioMime consists of an encoder and a conditional decoder. The decoder takes either an encoded latent or a standard normal sample as an input z and outputs a new sample \tilde{x} . The output \tilde{x} reflects the learned generative factors of the desired biophysical system state, the specified conditions c_s . The encoder is particularly useful when the objective is to conditionally modify the input data whilst retaining the generative effects of unspecified generative factors. **b**, BioMime is trained with an adversarial loss \mathcal{L}_{GAN} using a discriminator which seeks to distinguish between the generated samples \tilde{x} and the samples of the numerical simulator x_0 . Like the decoder, the discriminator is also conditioned on the specified conditions when given samples from the generator or the numerical simulator, meaning the generator must learn to generate a realistic MUAP that matches the input specified conditions. To further drive conditional behavior in the discriminator, the outputs of the numerical simulator x_0 are paired with the specified conditions which are either correct c_0 or incorrect c_r . To allow for *ab initio* generation and to stabilize training, an additional Kullback-Leibler divergence \mathcal{L}_{KL} term is minimized between z and a standard normal prior. Finally, we found empirically that adding a cycle-consistency loss \mathcal{L}_{cyclic} improved training stability and gave an increase in model performance (Supplementary Fig. S4). The input data from the numerical solutions x_0 with specified conditions c_0 are first transformed to match another set of specified conditions c_s and then transformed back to c_0 to calculate the cyclic loss. **c**, Rapid generation of dynamically evolving signals *ab initio*. A sample is taken from the prior and then continuously transformed over time using a sweep of the specified conditions.

Results

BioMime accurately mimics computationally expensive models

To demonstrate the ability of BioMime to capture a complex biophysical model, BioMime was trained to replicate an advanced numerical volume conductor model, which is used for generating surface electromyographic (sEMG) signals. We mainly focus on the example of replicating the volume conductor system in this paper. Another example in which BioMime is used to capture the relation between muscle lengths and joint angles in a biomechanical system can be found in Supplementary Text 5 and Fig. S6. Surface EMG, which is the summation of electrical potential signals from the active motor units in a

muscle, is a typical example of neurophysiological signals (15). It provides non-invasive information on neural activities and is commonly used for clinical/biomedical applications and human machine interfaces (16, 17, 18, 19). Modeling sEMG signals helps to uncover the underlying mechanisms of electrical potential field generation and propagation within human body and provides annotated dataset for training and validating signal processing techniques (20, 21).

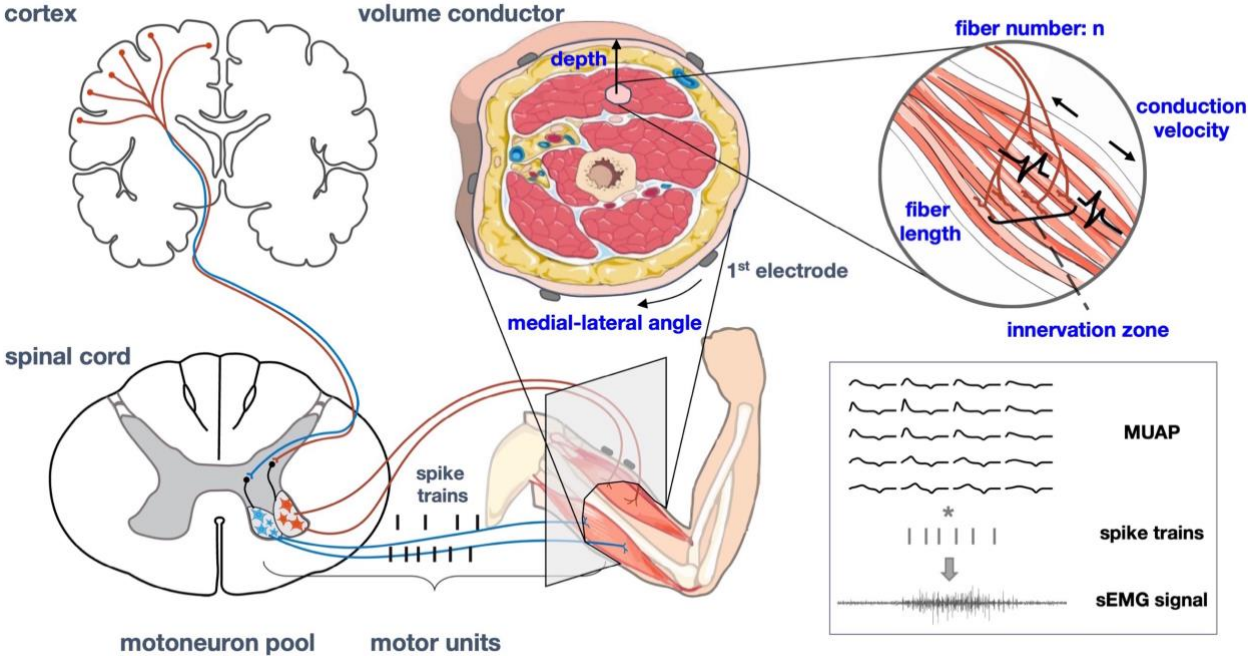


Fig. 2. Capturing a complex biophysical simulation. The effectiveness of BioMime is validated on a simulation of surface electromyogram (sEMG) signals recorded from a forearm. The sEMG signals represent the myoelectric output of motor neuron activities from the spinal cord and are detected by an array of electrodes placed on the skin above the muscles. Each spike from a specific motor neuron activates an associated pool of muscle fibers, where the combination of the motor neuron and the muscle fibers it controls is called a motor unit. The electrical potential field caused by the muscle activities is filtered by the volume conductor and sensed at the surface electrodes as the motor unit action potential (MUAP). Simulated MUAPs are convolved with the desired spike activities and then summed (with optional added gaussian noise) to build the simulated sEMG. For the outputs of the numerical simulation used to train BioMime, the bulk of MUAP variance is explained by six specified generative factors (printed in blue). These six factors are the specified conditions in the case of MUAP simulation.

Whilst numerical models of surface EMG generation have become highly advanced, they incur a huge computational burden when simulating the dynamic contractions, as the internal states of the model need to be continuously recalculated. This has proven to be a hindrance to the development of inverse models which can manage dynamic changes in the muscle (22), such as signals from a moving forearm used for prosthesis control. We proved that the proposed conditional generative model, BioMime, can learn from the teacher numerical model and accurately replicate the outputs of the numerical model.

The advanced numerical model we used to validate BioMime uses a finite element method to simulate motor unit action potentials (MUAPs), the basic component of EMG signal (21). As shown in Fig. 2, the shape of each MUAP waveform is dependent on multiple specified conditions, such as the location of the muscle fibers in the forearm (Fig. 3a).

BioMime was trained using a set of MUAPs generated by the numerical simulator. Each MUAP was labeled with the specific conditions used to generate the waveform. A held-out test set was used to validate the model. The test data was generated by using the same numerical model and the same forearm volume but include motor units that were not in the train data. The new motor units included unseen motor unit locations to BioMime and are used to test BioMime's ability to generate accurate MUAPs among all muscles (Details in Method). The testing was then done by taking a MUAP from the numerical simulator and using BioMime to transform the sample conditioned on another set of parameters in the test dataset. The output of BioMime was then compared to the equivalent output from the simulator. BioMime was able to consistently and accurately transform MUAPs based on the specified conditions, generating waveforms which were extremely similar in shape to the simulation equivalent (Fig. 3b). The mean normalized root mean square error (nRMSE) across all samples was 1.8% when evaluated on the held-out test set and there was equal performance across all six of the specified conditions (Fig. 3c).

An interesting result of conditioning the decoder is that the encoder outputs tended to lose the information about the specified conditions, analogous to semi-supervised disentanglement methods (23, 24). We investigated this effect with an informativeness metric (25), which measures how much information of the specified conditions are contained within the latent features. A non-linear regressor was used to inversely predict the specified conditions from the encoded waveform. We found that the latent features held very little information about the specified conditions, with a median informativeness score slightly above chance at 35.9% (Supplementary Table S2). This low informativeness metric indicates that the generative effects of the specified conditions were disentangled from those that were unspecified, i.e., not explicitly included during training. We speculate that this disentanglement improves the predictability of the model responses to the changes in the specified conditions by reducing the burden on the decoder.

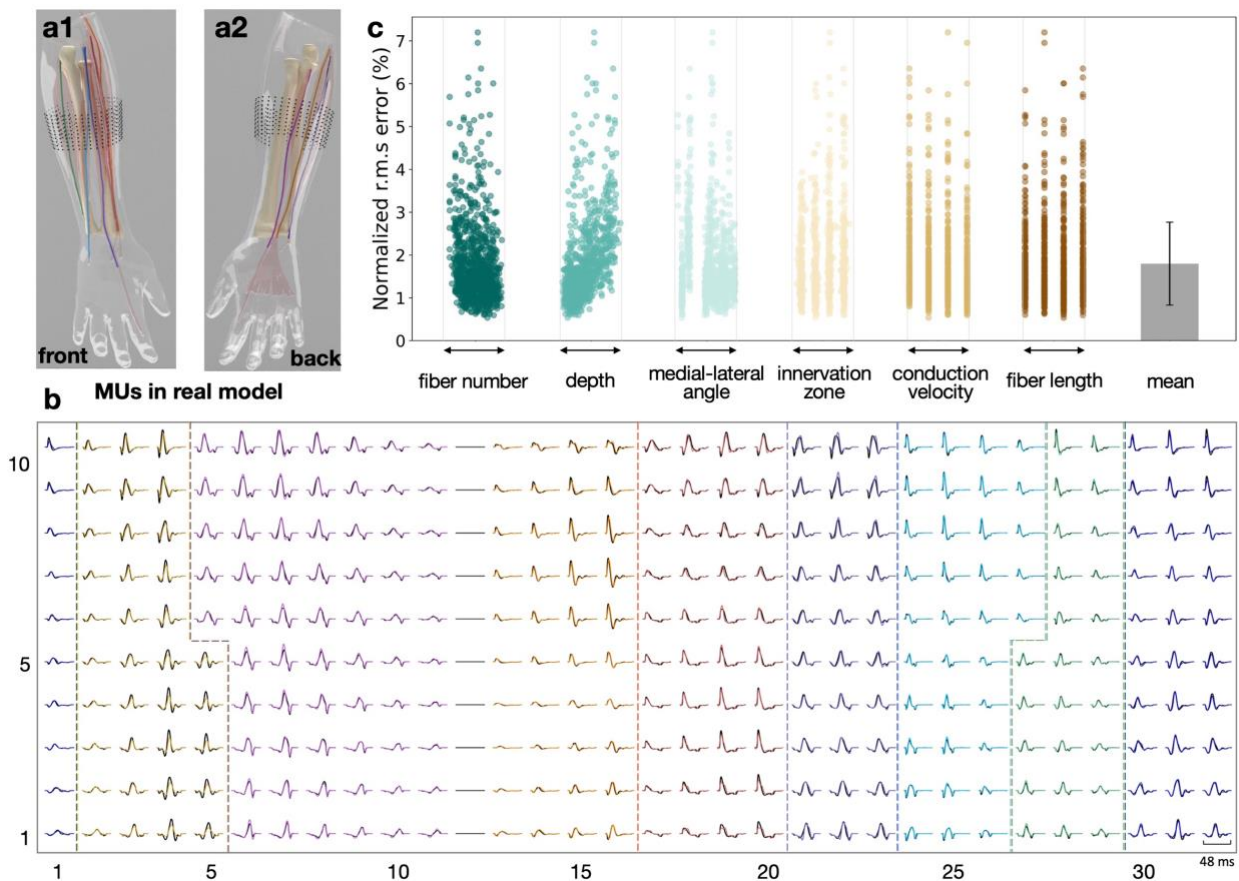


Fig. 3. BioMime accurately learns to mimic a biophysical simulation. **a**, Muscle fiber locations of the eight representative motor units (MUs) highlighted in different colors from front and back. Each MU is from a separate muscle in a realistic forearm volume conductor. The black dots represent the surface electrode array with 10×32 channels and the inter-electrode distance is 8mm. **b**, MUAP signals synthesized by conditionally transforming the action potentials of the eight MUs in **a**, compared with the ground truth in black lines. For each MU, only channels with large amplitudes are illustrated in sub-grids. These channels represent the electrodes that are physically closest to the MU. Sub-grids from different MUs are separated by dotted lines. The numbers beside and below the grid denote the indices of electrodes in row and in column, respectively. The shape of each transformed MUAP from BioMime closely matches its simulated counterpart. **c**, Normalized root mean square error in percentage between the outputs from BioMime and those from the numerical simulator across the six specified conditions and overall evaluated on the held-out test set. The normalized range of each condition's values is represented on the x-axis. The effect of all of the specified conditions on the simulations was closely mimicked by BioMime.

Predicting the outputs of a dynamically evolving system

To prove that BioMime could conditionally transform MUAPs by accurately interpolating among the internal states of the numerical simulator, we transformed MUAPs for all samples in the test dataset according to a sweep of the specified conditions. Three sets of conditions within the sweep matched the numerical dataset at equal distances along the swept paths. In other words, there were three ground truths that we can compare BioMime's outputs to. As shown in Fig. 4a, the simulated MUAPs changed continuously with the conditions and accurately matched the three ground truth MUAPs. The temporal

resolution of the interpolation can be ultra-high by simply increasing the number of time steps. As the specified conditions moved further away from the original values used to generate the waveform, the MUAP shape increasingly deviated away from the ground truth. However, the discrepancy was not large (nRMSE less than 2.0%) until the sweep intersected with the third ground truth (Fig. 4b), which was the sample with the generative factors most different from the original point. This means that even for situations where very high interpolation accuracies are desired during a dynamic traversal, a relatively small dataset from the computational expensive numerical simulator is sufficient.

We further visualized the distributions of the original dataset, interpolated BioMime transformations, and extrapolated BioMime transformations by using t-distributed stochastic neighbor embedding (t-SNE) dimensionality reduction (26) in Fig. 4c. The samples in the original dataset were grouped into small clusters, as the MUAPs in each muscle were highly similar. The waveforms generated by interpolating the specified conditions closely matched the distribution of the MUAPs from the original simulation. MUAPs generated by BioMime using specified conditions outside of those in the training set generally remained close to the original distribution until the specified conditions had deviated by a relative difference greater than 60%. This again demonstrates that BioMime is able to expand the data space whilst keeping the generation accuracy as well.

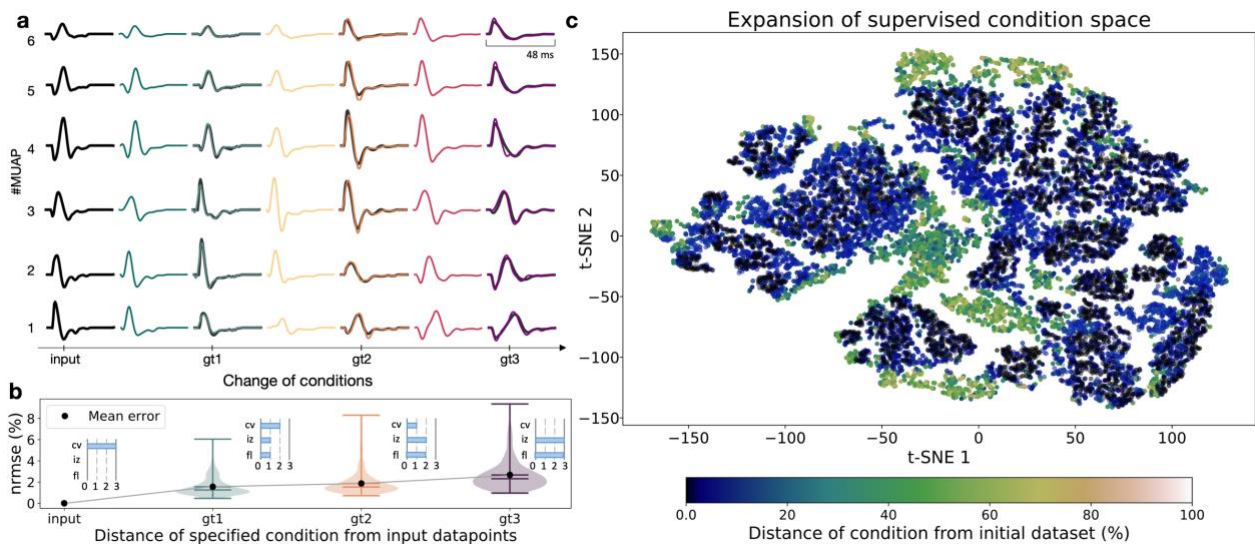


Fig. 4. BioMime can predictively interpolate and extrapolate between simulation conditions and beyond. **a**, A set of BioMime-transformed MUAPs sampled from a continuous sweep of specified conditions. The original MUAPs in the dataset were encoded and then continuously transformed away from their origins (x-axis tick label of ‘input’). As the specified conditions were continuously traversed, the MUAPs occasionally intersected with the generative factors from the numerical simulator (displayed as superimposed black lines, x-axis tick labels of ‘gt1’, ‘gt2’, and ‘gt3’), which can be used as a ground truth. Fiber density and MU location were kept constant while the other three parameters (conduction velocity, cv, innervation zone location, iz, and fiber length, fl) were continuously morphed away from the input conditions. The normalized values of these three parameters were displayed in the insets of **b**. **b**, Mean normalized root mean squared error of the BioMime-transformed MUAPs compared to their ground truth counterparts from the test set during the traversal in **a**. The predictive error of BioMime increased as the specified conditions moved further away from their origin.

BioMime is able to compensate for large moves away from the original conditions before the error starts to rise. **c**, A t-SNE projection of the MUAPs from the original simulation (black), interpolated BioMime transformations (blue) and extrapolated BioMime transformations beyond the specified conditions in the training set with color set by Euclidean distance from these conditions. The distribution of the interpolated MUAPs closely matched those from the original simulation, whilst the extrapolated MUAPs only started to deviate at relative distances greater than 60% from the ranges of specified conditions in the training set.

Inexpensively simulating a dynamic human biophysical system

Once trained, BioMime is able to rapidly generate outputs using any variety of reasonable conditions. Synthesizing hundreds of MUAPs within one muscle under one condition takes BioMime 0.287 seconds, which is two orders of magnitude faster than the state-of-the-art numerical model (30.8 seconds) in optimal conditions (21). When huge amounts of data are required for optimizing subject-specific parameters with grid searching, the time for generating MUAPs under 256,000 conditions is approximately 92 days by using the numerical model. By contrast, it takes BioMime 20 hours to simulate the same amount of data, with an addition of 12 days for using the numerical model to prepare for the dataset and training and testing the model on a sufficient subset of conditions. Further simulations would progressively increase the computational advantage of BioMime with respect to the numerical solution. Detailed comparison of runtimes between BioMime and the numerical model can be found in Supplementary Text 3 and Table S3.

Such low computational burden allows BioMime to produce continuous outputs of signals that capture the dynamics of the physical system. To demonstrate the utility of BioMime as a method of converting a static biophysical simulation into a dynamic one, the trained model was used to simulate sEMG signals from the outputs of a musculoskeletal model during finger and wrist movements (Fig. 5). We defined the movements of the musculoskeletal model by interpolating between four gestures, including palm extension, hand grasp, wrist flexion, and wrist extension (Fig. 5a). Details of the musculoskeletal model are described in Materials and Methods.

MUAPs from the eight forearm muscles in the numerical dataset were continuously transformed given the muscle length profiles from the musculoskeletal model. As only one specified condition, the muscle length, was changed during the transformation, the variation in the MUAP waveforms is mainly reflected in the duration of the waveform and the end-fiber effects, a complex interaction that is correctly predicted by BioMime (Fig. 5b). When more parameters can be tracked during the movement, BioMime will predict MUAPs that reflect a more realistic variation. To give a preliminary example, under an assumption that muscle volumes are constant during the movement (27), current source propagation velocity and MU depth can be tracked consistently with the changes of muscle length. MUAPs generated by BioMime under the changes of these three parameters exhibit more dramatic variations in waveforms (details are in Supplementary Text 4 and Fig. S5).

The library of the transformed MUAPs was then convolved with a set of motor neuron spike trains that represent a trapezoidal activation of flexors and extensors (Fig. 5d). We used trapezoidal activation since it is commonly used in the protocols for sEMG recordings. During the grip and wrist flexion, the flexors reached an excitation level of 60% maximum voluntary contraction (MVC). During the grip and wrist extension, the

extensors were activated with the same excitation level. Finally, the individual MU activities for each electrode channel were summed to give the final sEMG activity (Fig. 5e). This full-spectrum simulation is prohibitively time-consuming using numerical methods due to the computational cost of simulating hundreds of MUAPs at discretized stages of the movement. Simulating MUAPs during the 12-second movement with 50 Hz took the numerical model 5.2 hours. By contrast, it took 2.87 minutes for BioMime to simulate the same amount of data.

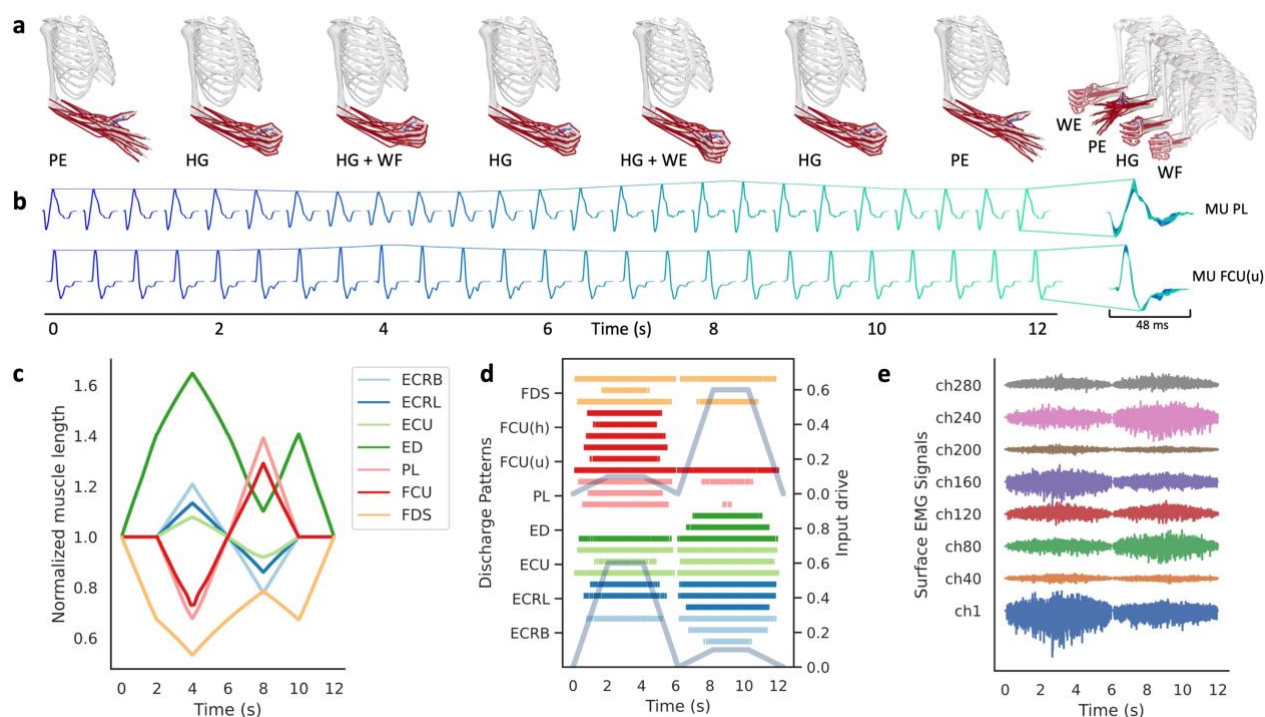


Fig. 5. BioMime can be used to mimic the dynamic changes of a biophysical system that matches the mechanical movements of a musculoskeletal model. **a**, Sequence of the movements. PE, palm extension; HG, hand grasp; WF, wrist flexion; WE, wrist extension. **b**, Two representative MUAPs generated by BioMime, which are continuously morphed using the muscle length profiles given by the musculoskeletal model. The upper MUAP is from Palmaris longus, PL and the lower MUAP is from the ulnar head of Flexor carpi ulnaris, FCU(u). The lines that connect the peak of MUAPs show the changes in MUAP amplitude. The MUAPs do not show extreme variations. This is expected as only one specified condition, the muscle length, is changed during the transformation. **c**, Normalized muscle length profiles from the musculoskeletal model. ECRB, Extensor carpi radialis brevis; ECRL, Extensor carpi radialis longus; ECU, Extensor carpi ulnaris; ED, Extensor digitorum; PL, Palmaris longus; FCU(u/h), Flexor carpi ulnaris (ulnar head/humeral head); FDS, Flexor digitorum superficialis. **d**, Representative discharge patterns of three motor units in each muscle. The motor unit spike trains were produced by the motoneuron pool model in (28) by simulating a trapezoidal activation of the flexors and the extensors. The activations of the flexor group (FDS, FCU(h), FCU(u), PL) and the extensor group (ED, ECU, ECRL, ECRB) are displayed. **e**, Simulated surface EMG signals in eight channels. This complex dynamic simulation is only possible due to the low computational cost of the hundreds of MUAP transformations conducted by BioMime.

Discussion

Humans are in nature dynamic systems. Computationally feasible methods are needed to better reflect this fact in biophysical simulations. By transferring the knowledge of numerical simulations to a conditional generative model, we demonstrate that the cost associated with simulating an evolving biophysical system can be largely mitigated without losing the prediction fidelity. With the correct architecture design, such models can act as both a rapid way to transform existing simulations to reflect new system states and as *de novo* generators for new data.

An example of a conditional generative model, BioMime, was demonstrated to generalizably and accurately learn the outputs of a teacher numerical simulator. Such advanced numerical simulators are commonly defined by a large number of differential equations which describe a complex system. BioMime was further able to continuously interpolate between the system states of the numerical simulator. This allows a rapid and robust generation of dynamic biophysical outputs that closely tracked those of the teacher finite element method-based simulation. In practice, generating data using BioMime was two orders of magnitude faster than using the numerical simulator. This efficiency provides feasible solutions to simulate a large amount of data under a grid of parameters, which will benefit parameter identification by grid searching, for example, to localize motor units within the muscles. The computational efficiency provided by BioMime also allows us to demonstrate the first practical model for simulating the myoelectric output of a moving forearm during a realistic hand and wrist movement. In the field of neurophysiological signal decomposition, there is a clear need for such simulations that capture the effect of dynamic changes to the volume conductor, which has so far proved a bottleneck to the development and validation of source separation algorithms that can operate on this highly non-stationary signal (22). The proposed methodology goes some way in meeting such a demand.

There is no requirement that BioMime be trained on the outputs of only one system. Here, we showed a feasible implementation of multi-domain simulations by feeding BioMime with the outputs of a musculoskeletal model during dynamic movements. This enables the exploration of neuromusculoskeletal mechanisms from both bioelectrical and biomechanical perspectives, the first step to interactively studying motoneuron activities and the movements driven by these activities (7). Combining BioMime with musculoskeletal modeling may also shed light on how to improve the performance of embodied agents in action-perception loops by providing the feedback of neuron activities during the movement. The computational burden of such full-spectrum simulations of biophysical systems is massive, which precludes the modeling of a range of movements with small time steps. However, this becomes possible by training conditional generative models like BioMime to effectively merge the outputs of the component simulations.

Another application is to use BioMime as a surrogate model of its simulation counterpart for the purposes of sensitivity analysis and parameter identification, which would otherwise be extremely computationally expensive (examples in Supplementary Text 3 and 4). An important feature of BioMime is that it is differentiable while the numerical model is not. Therefore, BioMime can be used as a forward surrogate model in an end-to-end optimization pipeline. This is expected to benefit solving inverse problems (29, 30), for example from EMG data or motions to spike trains or physiological parameters. Furthermore, if the simulation of the electrical generation process is part of a larger model, for example simulation from the motoneuron activities in a cellular level to the changes of

physiological parameters and finally to the electric potential field, a differentiable and computationally efficient forward model is required for an end-to-end optimization. BioMime provides a promising solution to approximating this complicated forward process.

The main disadvantage of using a conditional generative model for simulation is that it is reliant on the quality and quantity of the training data, although this is the case with any method of supervised or unsupervised machine learning. BioMime was trained on the dataset generated by an advanced numerical forearm model with a few condition changes. Since only one 3D model was included, BioMime embeds the variances of the immeasurable features of this forearm model into the unspecified conditions, as a “digital twin” of the individual’s forearm. Thus, the synthesized outputs are closely clustered with the samples in the original dataset. When more subject’s models are available in the dataset, the variance of the unspecified conditions increases. A future direction of research would be to explore the potential of BioMime on capturing the increased variance across subjects. We would expect combining the current training pipeline and transfer learning to be a possible solution.

It is important to emphasize that the methods outlined in this paper are designed to augment and approximate, rather than replace, high-quality numerical modelings. In many biophysical domains, the dynamic changes in system parameters in response to some perturbations remain poorly characterized, which restricts the utility of BioMime for simulating such systems. This is particularly true when modeling dynamic changes in a volume conductor for generating sEMG signals. While we attempted to carefully estimate the likely parameter changes during a forearm movement by using the musculoskeletal model, only muscle lengths can be tracked, which limits the precise restoration of MUAP changes. There is also a dearth of such information in the literature. We hope that the promise offered by conditional generative models in capturing the dynamic systems will further stimulate research in this direction, which will in turn improve the generation accuracy of BioMime. With better understanding of the volume conductor system and more applicable *in vivo* measurements, future investigation will be to compare BioMime’s simulation during dynamic movements with experimental EMG data.

Contemporary methods of biophysical simulation continue to offer a range of opportunities to both test physiological hypotheses and as a test bed for medical technologies. High representational-capacity generative modeling, such as the methods described in this paper, offers an enormously flexible opportunity for leveraging the domain knowledge contained within these complex systems. We anticipate that the pipeline of a back-end numerical model and a front-end generative model will become increasingly common in future simulation design, and we look forward to the corresponding expansion in dynamic simulations that these techniques will enable.

Materials and Methods

Data Preparation

We used an advanced finite element-based numerical model with a realistic forearm anatomy provided by the Neurodec software (21) to prepare the dataset (Supplementary Text 1 and Fig. S2). To simulate the motor unit action potentials with sufficient variations of conditions, a total of 1,500 motor units were randomly generated within eight forearm muscles. The eight muscles include the superficial muscles in the flexors and extensors of forearm. Those muscles are of most interest in studying forearm movement and contribute

the most to the simulated surface EMG signals due to their superficial locations. Each motor unit controlled a bundle of muscle fibers that clustered within a sub-volume of the muscle (Fig. 2). Six factors of variations that explained the bulk of MUAPs were defined as the specified conditions, covering the properties of current sources, motor units, and the volume conductor.

For each MU, the action potential templates under 256 conditions were generated, which were the combinations of four fiber densities (200, 266, 333, 400 fibers per mm^2), four current source propagation velocities (3.0, 3.5, 4.0, 4.5 m/s), four innervation zone positions (0.4, 0.46, 0.53, 0.6), and four fiber lengths in ratio (0.85, 0.95, 1.05, 1.15). Note that rather than directly using the fiber density as one of the conditions, we used the number of muscle fibers in each MU, such that this condition changed more continuously. The other two specified conditions are the depth and the medial-lateral position of the MU center, which was defined as the geometric center of all the muscle fibers it controlled. The six specified conditions were linearly normalized between 0.5 and 1. The influences of the six conditions on the MUAP attributes are visualized in Supplementary Fig. S3.

There were a total of 384,000 samples in this original dataset. Considering that the most unseen conditions come with different motor unit locations, we divide the dataset into the training dataset and the testing dataset by the motor units. For each muscle, 75% of MUs were randomly selected as the training set (288,000 samples) and the others as the held-out test set (96,000 samples). The MUAP templates were simulated with a bracelet of 10×32 electrodes with inter-electrode distance of 8 mm, which covered the bellies of the forearm muscles. The templates were represented as matrices with size $10 \times 32 \times T$. The number of time samples T varied among muscles due to the different fiber lengths and the current source propagation velocities. During the preprocessing of the MUAP data, the signals were first downsampled to 2,000 Hz. Finally, the signals were cut to a common length of 96 temporal samples (48 ms).

To test the ability of BioMime to adapt with better understandings of the forearm system, a new dataset was generated by using the same numerical model with one more condition, fat conductivity. Fat conductivity is an important subject-specific physical parameter that is difficult to measure *in vivo* but has an impact on the volume conduction effect (influence visualized in Supplementary Fig. S3). It was discretized to five steps between 0.024 and 0.215 S/m and normalized between 0.5 and 1. All the other parameters were the same as in the original dataset, which leads to a total of 1,920,000 samples. The training dataset (75% samples) and the testing dataset (25% samples) were divided by MU (same in the original dataset) to test the performance of the model when simulating motor units at unseen locations. Electrode configurations and the processing of MUAP templates were the same as in the original dataset.

Model Architecture

The proposed deep latent variable model, BioMime, takes the form of a probabilistic autoencoder architecture with an encoder and decoder network (Supplementary Table S1). The encoder network consists of five convolutional layers, each of which includes a 3D convolution with kernel size 3 followed by a 1×1 convolution with a skip connection. A parametric rectified linear unit activation (PReLU) operation is performed after each convolution layer. The convolutional output is then flattened and passed to two linear layers, which estimate the sufficient statistics of the approximate posterior, mean and variance, respectively. During training, the approximate posterior is sampled by the

reparameterization trick. During inference, the expectation of the posterior is used as the latent representation (Supplementary Algorithm 2) for transforming the input samples, whilst for *ab initio* generation, the latent representations are taken from a gaussian prior with zero mean and identity covariance (Supplementary Algorithm 3). The latent representation is then concatenated with a 64-dimensional learned linear projection of the six specified conditions before being passed to the decoder.

The decoder consists of four convolutions followed by two upscaling blocks. Each upscaling block consists of a time-scaling module, a 3D convolution, and a 1×1 convolution in sequence. The time-scaling module is a mean pooling/unpooling bank with learned weights (Supplementary Fig. S1), specialized for dilating or compressing the time sequences, which is essential in modeling physiological signals but computationally expensive to achieve through many convolutional operations. Inspired by the dynamic convolution in (31) and the multi-scale spatial pooling in (32), the time-scaling module uses a series of experts e_k with different scaling factors to dilate or compress the inputs, conditioned on the specified conditions \mathbf{c}_s . The contribution of each expert is modulated by a scalar weight, which is the output of a three-layer multilayer perceptron with the six specified conditions as input:

$$y = \sum_k \pi_k(\mathbf{c}_s) e_k(\mathbf{x})$$

$$s. t. 0 \leq \pi_k(\mathbf{c}_s) \leq 1, \sum_k \pi_k(\mathbf{c}_s) = 1 \quad (1)$$

where $\pi_k(\mathbf{c}_s)$ is the weight of the k th expert conditioned on the desired states \mathbf{c}_s . In this study, we used eight experts with scaling factors linearly spaced from 0.25 to 2.0, which showed optimal performance in both convergence and reconstruction accuracy (Supplementary Fig. S4).

Training Pipeline

Whilst BioMime has a deep latent variable architecture similar to a VAE, it is not trained variationally. Instead, we found that a conditional adversarial method gave the best performance. The output of BioMime is inspected by a conditional discriminator network of the similar architecture as the encoder, trained to identify whether samples are from the original dataset or generated by BioMime. Conditioning was performed by concatenating the output of the first convolutional layer of the discriminator with the specified conditions.

The goals of training BioMime are to 1) produce novel data samples that are realistic enough to fool the discriminator and 2) enable generation by both sampling from a prior distribution and by encoding an existing sample. These are achieved by optimizing the following objective function:

$$\mathcal{L}_G = \lambda_1 \mathcal{L}_{GAN} + \lambda_2 \mathcal{L}_{KL} + \lambda_3 \mathcal{L}_{cyclic} \quad (2)$$

The first term \mathcal{L}_{GAN} is an adversarial loss, which evaluates the performance of BioMime using the conditional discriminator. The second term \mathcal{L}_{KL} is the Kullback-Leibler divergence ($D_{KL}(\cdot \parallel \cdot)$) between the predicted distribution of the latent feature and the standard normal distribution $N(0, 1)$. Minimizing \mathcal{L}_{KL} regularizes the latent space to approach $N(0, 1)$. This enables the model to generate new data by sampling from the prior. An additional cycle-consistency loss \mathcal{L}_{cyclic} is included to improve training stability and generation accuracy (Supplementary Fig. S4), which is the mean-squared error

between the input sample and the reversed sample (Fig. 1b). In our experiments, the hyper-parameters λ_1 was set 10, λ_2 was an annealing weight (33) increased from 0 to 0.05 in 30,000 iterations, and λ_3 was set 0.5. Comparisons of constant, logistic, and linear KL divergence schedules are shown in Supplementary Fig. S4.

The objective of the discriminator is to differentiate the data samples produced by the generator from those in the original dataset whilst also detecting whether the samples match the specific conditions. This is done by minimizing:

$$\begin{aligned} \mathcal{L}_D = & -\mathbb{E}_x[\log D(\mathbf{x}, \mathbf{c}_s)] - \mathbb{E}_x[\log(1 - D(\mathbf{x}, \mathbf{c}_r))] * 0.5 \\ & - \mathbb{E}_x[\log(1 - D(G(\mathbf{x}, \mathbf{c}_s), \mathbf{c}_s))] * 0.5 \end{aligned} \quad (3)$$

In this way, the discriminator only predicts an input as real when the sample \mathbf{x} is realistic and matches the desired conditions \mathbf{c}_s . Real samples \mathbf{x} with random conditions \mathbf{c}_r or synthesized samples $G(\mathbf{x}, \mathbf{c}_s)$ with matched conditions \mathbf{c}_s are predicted as fake.

Training Process

The ratio between the discriminator and the generator updates was set 1:1 (Supplementary Algorithm 1). The discriminator and the generator were trained on the original dataset for 45 epochs (405,000 iterations) with RMSprop optimizer and learning rate of 1×10^{-5} . The number of input signals in each training mini-batch was set to 32. Training took 120 hours (~5 days) on an NVIDIA RTX 2080Ti. The best models of the discriminator and the generator were used as pretrained models and were fine-tuned on the new dataset for 6 epochs (270,000 iterations). Adam optimizer was used with a cosine annealing learning rate from 1×10^{-4} to 1×10^{-5} . Fine-tuning took 54 hours on an NVIDIA RTX 2080 Ti.

Model Validation

To validate the model, we evaluated the ability of BioMime to transform the existing MUAP templates to new sets of simulation parameters. This was performed by optimizing the model on the training dataset and evaluating its performance on the held-out test set. We randomly selected two data samples with the same unspecified generative factors and transformed the first sample to match the second sample's specified conditions. The generation accuracy was evaluated by the normalized root mean square between the predicted MUAP and the ground truth MUAP.

Musculoskeletal Model

To simulate MUAPs and the accumulated muscle activities during a realistic movement, we fed BioMime with a sequence of continuously changed physiological parameters. The length of each muscle was computed by an open-source musculoskeletal model (34) with a hand, wrist, and forearm in OpenSim (35). The model includes 23 independent degrees of freedom and 43 hill-type muscle-tendon actuators that represent the intrinsic muscles of the hand, the extrinsic muscles of the hand, and the primary wrist muscles. We defined four gestures, palm extension (PE), hand grasp (HG), wrist flexion (WF), and wrist extension (WE) by setting the joint angles. The musculoskeletal model was driven by the interpolated joint angles. Starting from the gesture of palm extension, the model performed the following (combinations of) gestures in sequence: hand grasp, hand grasp and wrist flexion, hand grasp, hand grasp and wrist extension, hand grasp, and palm extension. Each movement took 2 seconds, thus 12 seconds in total. The profiles of equilibrium muscle lengths were computed at 50 Hz frequency. The muscle lengths were first normalized to the lengths at the start position (PE) before fed into BioMime to simulate dynamic MUAP waveforms.

Informatic Analyses

Normalized root mean square error To quantify the accuracy of the generated signals compared with the ground truth, the normalized root mean square error was used as a metric:

$$\text{nRMSE} = \frac{\sqrt{\sum_{h,w,t} (x_{h,w,t} - \tilde{x}_{h,w,t})^2 / H/W/T}}{x_{max} - x_{min}} \quad (3)$$

where x and \tilde{x} indicate the ground truth MUAP from the numerical model and the synthesized MUAP by BioMime. The variables h , w , t are the summation over the rows and columns of the electrode and the time samples, with the total number H , W , and T , respectively. x_{max} and x_{min} are the maximum and minimum values of the sample. The normalized root mean square error is often expressed as a percentage, with a lower value indicating a less residual variance for the model and a higher generation accuracy. We empirically found that a nRMSE less than 2.0% indicates a good generation with few differences between the generated data and the ground truth data.

t-distributed stochastic neighbor embedding (t-SNE) To visualize the implicit structure of the MUAP data, we used t-SNE to project the signals to a low-dimensional submanifold. The scikit-learn t-SNE module was used with default settings (dimension of the embedded space 2, perplexity 30, learning rate 200, maximum number of iterations 1000, initialization of embedding using principal component analysis) (36). The samples were visualized in the coordinates given by t-SNE, where similar samples were close together in the submanifold.

Informativeness score We explored the amount of information of the specified conditions embedded in the latent representations of the generator. The informativeness of the latent vector z about the i^{th} generative factor c_{si} can be quantified by the prediction accuracy $P(c_{si}, f(z))$, where P is an accuracy metric and f is a regressor (25). The informativeness depends on 1) the regressor's capability to extract information from the latent representations and 2) the way the specified conditions are embedded in the latent features, e.g., disentanglement of the specified conditions in the representations will make the regression easier.

We used multilayer perceptron with non-linear activation functions to predict c_{si} from z . The prediction accuracy was measured as the percentage of correctly predicted samples. A sample was regarded as correct when the relative error between the predicted and real conditions was within a threshold. For instance, with the threshold of 0.05, a sample with ground truth condition a will be evaluated as correct if the predicted condition is between $0.95a \sim 1.05a$. We chose ten threshold levels, linearly spaced from 0.01 to 0.10, and calculated the average accuracy as the informativeness score (Supplementary Table S2).

References

1. W. Gerstner, H. Sprekeler, G. Deco, Theory and simulation in neuroscience. *Science* **338**, 60–65 (2012).
2. E. Halilaj, A. Rajagopal, M. Fiterau, J. L. Hicks, T. J. Hastie, S. L. Delp, Machine learning in human movement biomechanics: Best practices, common pitfalls, and new opportunities. *J. biomechanics* **81**, 1–11 (2018).
3. A. L. Hodgkin, A. F. Huxley, A quantitative description of membrane current and its application to conduction and excitation in nerve. *The J. Physiol.* **117**, 500 (1952).
4. M. Breakspear, Dynamic models of large-scale brain activity. *Nat. Neurosci.* **20**, 340–352 (2017).

5. D. Baby, A. Van Den Broucke, S. Verhulst, A convolutional neural-network model of human cochlear mechanics and filter tuning for real-time applications. *Nat. Mach. Intell.* **3**, 134–143 (2021).
6. M. Fuchs, R. Drenckhahn, H. Wischmann, M. Wagner, An improved boundary element method for realistic volume-conductor modeling. *IEEE Transactions on Biomed. Eng.* **45**, 980–997 (1998).
7. V. Caggiano, H. Wang, G. Durandau, M. Sartori, V. Kumar, Myosuite: A contact-rich simulation suite for musculoskeletal motor control in Learning for Dynamics and Control Conference. (PMLR), pp. 492–507 (2022).
8. D. Pereira Botelho, K. Curran, M. M. Lowery, Anatomically accurate model of EMG during index finger flexion and abduction derived from diffusion tensor imaging. *PLoS Comput. Biol.* **15**, e1007267 (2019).
9. A. Erdemir, Open knee: open source modeling and simulation in knee biomechanics. *The J. Knee Surg.* **29**, 107–116 (2016).
10. A. Marrel, N. Perot, C. Mottet, Development of a surrogate model and sensitivity analysis for spatio-temporal numerical simulators. *Stoch. Environ. Res. Risk Assess.* **29**, 959–974 (2015).
11. F. Zhuang, et al., A comprehensive survey on transfer learning. *Proc. IEEE* **109**, 43–76 (2020).
12. Y. Pu, Z. Gan, R. Henao, X. Yuan, C. Li, A. Stevens, L. Carin, Variational autoencoder for deep learning of images, labels and captions. *Adv. Neural Inf. Process. Syst.* **29** (2016).
13. X. Yan, J. Yang, K. Sohn, H. Lee, Attribute2image: Conditional image generation from visual attributes in European Conference on Computer Vision. (Springer), pp. 776–791 (2016).
14. N. W. Gebauer, M. Gastegger, S. S. Hessmann, K. R. Müller, K. T. Schütt, Inverse design of 3d molecular structures with conditional generative neural networks. *Nat. Commun.* **13**, 1–11 (2022).
15. R. Merletti, D. Farina, *Surface electromyography: physiology, engineering, and applications.* (John Wiley & Sons), (2016).
16. D. Farina, N. Jiang, H. Rehbaum, A. Holobar, B. Graimann, H. Dietl, O.C. Aszmann, The extraction of neural information from the surface EMG for the control of upper-limb prostheses: emerging avenues and challenges. *IEEE Transactions on Neural Syst. Rehabil. Eng.* **22**, 797–809 (2014).
17. V. Ruonala, A. Meigal, S. M. Rissanen, O. Airaksinen, M. Kankaanpää, P. A. Karjalainen, EMG signal morphology and kinematic parameters in essential tremor and Parkinson’s disease patients. *J. Electromyogr. Kinesiol.* **24**, 300–306 (2014).
18. T. S. Saponas, D. S. Tan, D. Morris, R. Balakrishnan, Demonstrating the feasibility of using forearm electromyography for muscle-computer interfaces in Proceedings of the SIGCHI Conference on Human Factors in Computing Systems. pp. 515–524 (2008).
19. D. Xiong, D. Zhang, X. Zhao, Y. Zhao, Deep learning for EMG-based human-machine interaction: a review. *IEEE/CAA J. Autom. Sinica* **8**, 512–533 (2021).
20. D. Farina, F. Negro, M. Gazzoni, R. M. Enoka, Detecting the unique representation of motor-unit action potentials in the surface electromyogram. *J. Neurophysiol.* **100**, 1223–1233 (2008).

21. K. Maksymenko, A. K. Clarke, I. Mendez Guerra, S. Deslauriers-Gauthier, D. Farina, A myoelectric digital twin for fast and realistic modelling in deep learning. *Nat. Commun.* **14**, 1600 (2023).
22. V. Glaser, A. Holobar, Motor unit identification from high-density surface electromyograms in repeated dynamic muscle contractions. *IEEE Transactions on Neural Syst. Rehabil. Eng.* **27**, 66–75 (2018).
23. P. K. Gyawali, Z. Li, S. Ghimire, L. Wang, Semi-supervised learning by disentangling and selfensembling over stochastic latent space in International Conference on Medical Image Computing and Computer-Assisted Intervention. (Springer), pp. 766–774 (2019).
24. T. Wang, Z. Yue, J. Huang, Q. Sun, H. Zhang, Self-supervised learning disentangled group representation as feature. *Adv. Neural Inf. Process. Syst.* **34**, 18225–18240 (2021).
25. C. Eastwood, C. K. Williams, A framework for the quantitative evaluation of disentangled representations in International Conference on Learning Representations. (2018).
26. L. Van der Maaten, G. Hinton, Visualizing data using t-SNE. *J. Mach. Learn. Res.* **9** (2008).
27. L. Mesin, M. Joubert, T. Hanekom, R. Merletti, D. Farina, A finite element model for describing the effect of muscle shortening on surface EMG. *IEEE Transactions on Biomed. Eng.* **53**, 593–600 (2006).
28. A. J. Fuglevand, D. A. Winter, A. E. Patla, Models of recruitment and rate coding organization in motor-unit pools. *J. Neurophysiol.* **70**, 2470–2488 (1993).
29. D. Montes de Oca Zapiain, J. A. Stewart, R. Dingreville, Accelerating phase-field-based microstructure evolution predictions via surrogate models trained by machine learning methods. *npj Comput. Mater.* **7**, 1–11 (2021).
30. J. Granley, L. Relic, M. Beyeler, Hybrid neural autoencoders for stimulus encoding in visual and other sensory neuroprostheses in *Advances in Neural Information Processing Systems*. (2022).
31. Y. Chen, X. Dai, M. Liu, D. Chen, L. Yuan, Z. Liu, Dynamic convolution: Attention over convolution kernels in *Proceedings of the IEEE/CVF Conference on Computer Vision and Pattern Recognition*. pp. 11030–11039 (2020).
32. J. W. Chen, R. Wang, F. Ding, B. Liu, L. Jiao, J. Zhang, A convolutional neural network with parallel multi-scale spatial pooling to detect temporal changes in SAR images. *Remote. Sens.* **12**, 1619 (2020).
33. S. R. Bowman, L. Vilnis, O. Vinyals, A. M. Dai, R. Jozefowicz, S. Bengio, Generating sentences from a continuous space. *arXiv preprint arXiv:1511.06349* (2015).
34. D. C. McFarland, B. I. Binder-Markey, J. A. Nichols, S. J. Wohlman, M. de Bruin, W. M. Murray, A musculoskeletal model of the hand and wrist capable of simulating functional tasks. *IEEE Transactions on Biomed. Eng.* **70**, 1424-1435, (2022).
35. S. L. Delp, et al., Opensim: open-source software to create and analyze dynamic simulations of movement. *IEEE Transactions on Biomed. Eng. Scikit-learn: Machine Learning in Python*
36. F. Pedregosa, et al., *Scikit-learn: Machine Learning in Python*. *J. Mach. Learn. Res.* **12**, 2825–2830 (2011).

37. S. Bai, J. Z. Kolter, V. Koltun, An empirical evaluation of generic convolutional and recurrent networks for sequence modeling. arXiv preprint arXiv:1803.01271 (2018).
38. E. Petersen, P. Rostalski, A comprehensive mathematical model of motor unit pool organization, surface electromyography, and force generation. *Front. Physiol.* **10**, 176 (2019).
39. A. Hyvärinen, E. Oja, A fast fixed-point algorithm for independent component analysis. *Neural Comput.* **9**, 1483–1492 (1997).
40. B. Grandi Sgambato, et al., High performance wearable ultrasound as a human machine interface for wrist and hand kinematic tracking. *TechRxiv* (2023).
41. R. Merletti, S. Muceli, Tutorial. Surface EMG detection in space and time: Best practices. *J. Electromyogr. Kinesiol.* **49**, 102363 (2019).

Acknowledgments

We would like to thank Pranav Mamidanna for the discussions and assistance in preparing for the musculoskeletal model. We acknowledge Bruno Grandi Sgambato for helping with the initial dataset for training the conditional generative model in biomechanical systems (Supplementary Text 5).

Funding:

National Natural Science Foundation of China (Grant No. 91948302, 52175021)
European Research Council Synergy Grant NaturalBionicS (contract 810346)
EPSRC Transformative Healthcare, NISNEM Technology (EP/T020970)
BBSRC, “Neural Commands for Fast Movements in the Primate Motor System” (NU-003743)

Author contributions:

Conceptualization: SM, AKC, DF
Methodology: SM, AKC, DF
Dataset Preparation: SM, KM, SD
Investigation: SM, AKC
Visualization: SM
Supervision: XS, XZ, DF
Writing—original draft: SM, AKC
Writing—review & editing: SM, AKC, DF

Competing interests: KM and SD are cofounders of the company Neurodec.

Data and materials availability: Code which implements the models used in this paper is available at <https://github.com/shihan-ma/BioMime> and is provided under the GNU General Public License v3.0. All data are available in the main text or the supplementary materials.

Supplementary Materials for

- **Human Biophysics as Network Weights: Conditional Generative Models for Dynamic Simulation**

Shihan Ma *et al.*

*Corresponding author. Email: d.farina@imperial.ac.uk and mexyzhu@sjtu.edu.cn

This PDF file includes:

Supplementary Text
Figs. S1 to S7
Tables S1 to S3
Algorithms S1 to S3

Supplementary Text

Supplementary Text 1: Numerical Simulation

Specified Conditions

The MUAP dataset consists of MUAP templates from eight forearm muscles generated by an advanced and realistic numerical model (21), as shown in Supplementary Fig. S2a. Both superficial flexors and extensors are included, i.e., Extensor carpi radialis bevis, Extensor carpi radialis longus, Palmaris longus, Flexor carpi ulnaris ulnar head, Flexor carpi ulnaris humeral head, Extensor carpi ulnaris, Extensor digitorum, Flexor digitorum superficialis, with 186, 204, 164, 205, 217, 180, 186, and 158 unique motor units (MUs), respectively. In total, we have 1,500 MUs in the dataset.

In each muscle, the fibers that belong to a single MU cluster within a sub-volume of the muscle. Here we define the center of a MU as the centroid of all the points of intersections between the fibers and the reference plane. The 2D location of a MU center is described by its depth and medial-lateral position (Supplementary Fig. S2b). The depth of a MU is defined as the closest distance between the MU center and the skin surface. The medial-lateral position of the MU is represented by the radian of the MU center with respect to the reference electrode, \widehat{AB} / p , where p is the perimeter of the cross-section.

For each MU, the action potential templates were generated under 256 conditions, which are the combinations of four fiber densities (200, 266, 333, 400 fibers per mm^2), four current source propagation velocities (3.0, 3.5, 4.0, 4.5 m/s), four innervation zone positions (0.4, 0.46, 0.53, 0.6), and four fiber lengths in ratio (0.85, 0.95, 1.05, 1.15). Consequently, there were a total of six well-defined conditions that can be manually modified. These conditions were linearly normalized between 0.5 and 1. The influences of the six conditions on the MUAPs are visualized in Supplementary Fig. S3, by generating MUAP templates using a cylindrical numerical model while individually changing each of the six conditions. We used the cylindrical model here as the 2D locations of the muscle fibers are difficult to change manually in the realistic numerical model. Note that rather than directly using the fiber density as one of the conditions, we used the number of muscle fibers in each MU, such that this condition changed more continuously.

Dataset with Changes of Fat Conductivity

To test the performance of BioMime to capture more physiological parameters of the forearm system, a new and larger dataset was generated by using the same numerical forearm model. The new dataset included one more parameter, fat conductivity. Fat conductivity is a subject-specific physiological parameter that shapes the surface detected potential field by changing the volume conduction effect. With lower conductivity, fat layer constrains the diffusion of electric currents and produces higher currents and higher voltages at the surface electrodes (39) (Influence shown in Supplementary Fig. S3). The fat conductivity was discretized into five steps between 0.024 and 0.215 S/m and normalized between 0.5 and 1. The numerical model was rerun for five times to generate the action potentials at the basis points for the five fat conductivities. All the other parameters were the same as in the original dataset. Therefore, seven specified conditions can be modified in the new dataset.

Supplementary Text 2: BioMime Model

Time-scaling Module

BioMime has an encoder-decoder structure. The encoder embeds the input samples into latent features while the decoder converts the latent features to the output signals conditioned on the desired system state. We found empirically that multiple layers of fractionally-strided convolutions in the decoder, which are commonly used in restoring images, could not accurately generate MUAP signals that match the expected system conditions (Supplementary Fig. S4). One possible reason is that simulating physiological signals requires the model to flexibly transform the long time sequence while traditional convolution filters have limitations when dealing with long distance relationships (37).

Inspired by the dynamic convolution in (31) and the multi-scale spatial pooling in (32), we proposed a time-scaling module, which is a temporal pooling/unpooling bank with learned weights specialized for dilating or compressing the time sequences in a large scale. A series of experts with different scaling factors are incorporated to endow the model with a dynamic scaling ability (Supplementary Fig. S1). Experts with scaling factors less than one compress the duration of the signal while experts with scaling factors larger than one dilate the signal. The compressed signals are padded with zeros at the end while the dilated ones are truncated to have the same size. The weights of the experts are projected from the specified conditions by a feedforward neural network (three linear layers with two activation layers) and are normalized by softmax, as the scale of the expected MUAP greatly relies on the specified conditions, e.g., deeper location of fibers within the muscle results in more attenuated signals.

We found that ranging the temporal scaling factors between 0.25 and 2.0 is sufficient for well transforming the MUAP signals of the forearm muscles. Increasing the number of experts introduces more scaling factors but also increases the training time. Time-scaling module with eight experts generated accurate signals within an acceptable training iteration (Supplementary Fig. S4). Therefore, eight experts were used in BioMime model.

Supplementary Text 3: Training Process

Choice of Hyper-parameters

There are three hyper-parameters in training BioMime, the weights of the three losses in the objective function. During training, we first empirically set all weights to 1.0 and adjusted the learning rate of the RMSprop optimizer to make sure all losses were continuously decreasing during training. We tried the learning rate of 1e-3, 1e-4, and 1e-5 and chose 1e-5. Then the weights of the loss functions were adjusted to improve the performance of BioMime. Since the adversarial loss is the primary loss that affects the quality of the simulated MUAPs, we set its weight to a high value, 5 and 10. The Kullback-Leibler divergence (KLD) loss is the regularization loss, so we set a small weight as 0.05 and 0.1. The cyclic loss is also important to improve the stability of training and improve the performance of BioMime, so we set its weight as 1.0 and 0.5. We used grid searching to find the best set of hyper-parameters. It is not required to train the whole epochs for each set of hyper- parameters during the grid searching. Usually, the losses during the first several epochs provide sufficient information for us to decide whether to keep this set of hyper-parameters or not. Finally, inspired by (33), we tried the annealing weights of KLD loss and found it improved the generation accuracy. The number of iterations for the annealing was empirically set 30,000.

Schedules of Kullback-Leibler (KL) Divergence Term

When trained with constant KL divergence term, the network converged slowly, and the generation accuracy was low. We suppose this is because the regularization of the latent space was strict, and thus the model was slow to capture the latent representations from the beginning of the training. We found that an annealing schedule for KL divergence loss (33), no matter linear or logistic, drove the model to converge faster and achieve higher prediction accuracy than with a constant weight (Supplementary Fig. S4). By starting from a small coefficient, the model focused on extracting the information from the input data and reconstructing the output, rather than regularizing the latent space that might interfere the learning process. As the weight increased, the model gradually regulated the latent features and reached a balance between the regularized space and the real space. The logistic and linear terms are formulated as follows:

$$w = \begin{cases} \frac{1}{1 + e^{-k \cdot (x - x_0)}}, & w \text{ in logistic form} \\ \frac{x}{N}, & w \text{ in linear form} \end{cases} \quad (1)$$

where x denotes the current iteration and the hyperparameters $k = 1$, $x_0 = 6$, and $N = 30,000$.

Fine-tuning on Dataset with Fat Conductivity

To save time and transfer the knowledge from BioMime's best model trained on the original dataset, we fine-tuned BioMime on a new dataset with one more specified condition (fat conductivity). The best models of the discriminator and the generator trained on the original dataset were used as pre-trained models. Adam optimizer was used with a cosine annealing learning rate from 1×10^{-4} to 1×10^{-5} . Fine-tuning took 6 epochs (270,000 iterations), that is 54 hours on a NVIDIA RTX 2080 Ti. The overall performance of BioMime on the new dataset is on

par with the original test data, showing the generation accuracy of 2% when evaluated with the normalized root mean square error on the held-out dataset. Representative examples of simulated MUAPs by BioMime and the ground truth from the numerical model are shown in Supplementary Fig. S7.

Comparison of Runtimes with Numerical Model

A comparison of runtimes for BioMime versus the numerical model is displayed in Supplementary Table S3. Although it took several days to prepare for BioMime’s dataset and to train the model, BioMime still has advantages from several aspects. Here we give examples to show BioMime’s computational benefit over the numerical model. And we want to emphasize that the numerical model we are comparing with is the state-of-the-art numerical model in simulating electrical potential field of physical systems (21).

We first explain how the numerical model generates MUAPs. The numerical model first solves the forward solution to calculate the electrical potentials at all basis points within the model (General forward solution in Table S3). Changing geometries of the volume conductor (e.g., fat thickness) or changing tissue conductivities require to recompute the forward solution. Then, the fibers in each muscle are distributed within a unit circle, assigned to the motor units, and projected to the muscle geometry (Preparation for the fiber basis points in Table S3). Changing fiber density or fiber geometry requires to regenerate fiber basis points. Rerunning the forward solution also requires regenerating fiber basis points. Lastly, MUAPs are simulated given the properties of the fibers in each MU (MUAP simulation in Table S3). The properties include fiber length, innervation zone, etc.

With the new BioMime that was fine-tuned on the new dataset with fat conductivity, we show examples that BioMime has the computational benefit over the teacher numerical model. BioMime is useful when a large number of simulation runs are required. For example, to perform sensitivity analysis to explore the behaviors of the system when the parameters are varying or to identify the optimum subject-specific parameters during grid searching. Identification of subject-specific parameters is important to build an accurate “digital twin” for an individual. Subject-specific parameters include fat conductivities, fiber density, etc. These parameters are difficult to measure but can be estimated by multiple simulations with grid searching. Consider one grid searching to identify the fiber density and fat conductivity for one specific subject. Assume that we discretize the fat conductivity to 10 steps, fiber density to 5 steps, fiber length to 8 steps, position of innervation zone to 8 steps, and current source conduction velocity to 8 steps. Running the grid searching for the 320 electrodes takes the numerical model:

$$(5*10*(2*60+8^3*30.8)+13*320)*10/3600/24 \approx 92.5 \text{ days} \quad (2)$$

Note that above, for each fiber density, we ran ten times of fiber basis generation to consider the effect of the randomness introduced by fiber points allocation (38).

Simulating the same amount of data takes BioMime $0.287 * 10 * 5 * 10 * 83 = 20.4$ hours. The old BioMime dataset includes 8 muscles, 4 fiber densities, 4 innervation zones, 4 conduction velocities, and 4 muscle lengths. Preparation for this dataset using the numerical model took (320

$* 13 + 4 * 8 * (2 * 60 + 64 * 30.8) / 3600 \approx 19.744$ hours. The new dataset that includes 5 fat conductivities requires rerunning the model for 5 times. The generation time is $5 * (320 * 13 + 4 * 8 * (2 * 60 + 64 * 30.8)) / 3600 \approx 98.72$ hours. Training the base BioMime with the old dataset took 120 hours. Fine-tuning the model on the new dataset took 6 epochs (9 hours per epoch), a total of 54 hours. In total, it took BioMime $19.744 + 98.72 + 120 + 54 + 20.4 = 312.864$ hours = 13 days to do this grid searching, which is much shorter than the 92.5 days taken by the numerical model.

The time for generating the dataset and training the model is constant. And the impact of this constant time is reduced with increasing use of BioMime since BioMime's inference time (0.287 s) is two orders of magnitude less than the numerical model (30.8 s). For example, simulating MUAPs during a movement (15 seconds, 50 Hz) takes the numerical model 6.4 hours while BioMime 3.58 minutes.

Numerical Model in Parallel as Baseline

Given the example above, it took the numerical model 92.5 days to simulate MUAPs under 256,000 conditions, in which the numerical model was reran for five times. In comparison, it took BioMime 13 days to simulate the same amount of data (with data preparation and training time). The numerical model needs to run on at least 11 workers in parallel to match the time by BioMime. The number of parallel workers (w) is solved by the following equation:

$$92.5 / w = (19.744 + 98.72) / 24 / w + (54 + 120 + 20.4) / 24 \quad (3)$$

However, it will be almost impossible for the numerical model to match BioMime in the simulation time for each new condition, even without the need to rerun the forward solution or regenerate the fiber basis. The numerical model needs to run on $30.8 / 0.287 = 107$ workers in parallel to match BioMime. In addition, BioMime can be trained in parallel on multiple GPUs, thus the constant time and the linear time can be further reduced.

Numerical Model in Parallel as Baseline

The hardware used in the numerical model is Processor AMD Ryzen 7 1700 Eight-Core Processor, 3000 Mhz, 8 Core(s), 16 Logical Processor(s), 32 GB RAM. BioMime was trained, tested, and fine-tuned on a machine equipped with a NVIDIA RTX 2080 Ti GPU and 128 Intel(R) Xeon(R) Platinum 8358P CPU cores running Ubuntu 20.04.

Supplementary Text 4: Application

Simulating Dynamic MUAPs with MSK Model

We demonstrated in the manuscript that BioMime can be integrated with musculoskeletal (MSK) models to simulate changes of MUAPs during a random movement. One of the specified conditions in BioMime, muscle length, was tracked by using OpenSim. Changes of muscle length were fed with BioMime to output dynamic MUAPs during the movement. Although it is difficult to track the other parameters during a movement, current source propagation velocity and MU depth can be approximated under some assumptions. If we assume that the volumes of the muscles are constant during the movement (27), the cross-section of muscle will change inversely with the muscle length. Assuming that current source propagation velocity changes proportionally with the muscle cross-sections and MU depth changes proportionally with the fiber diameter, these two parameters can be approximately tracked during the movement.

The changes of muscle length, current source conduction velocity, and MU depth during the same movement as in manuscript Fig. 5 are shown in Supplementary Fig. S5 c, d, and e. Two representative MUAPs (same in manuscript Fig. 5) were transformed by BioMime during the movement by changing only fiber length, changing fiber length and current source conduction velocity, and changing all of the three parameters (Supplementary Fig. S5 b). Changing the current source propagation velocity changes the duration of the MUAP while changing MU depth has a dramatic impact on the shapes of the waveforms, which is consistent with previous studies.

Supplementary Text 5: Conditional Generative Model in Biomechanical Systems

Here we provide another example to show that under the same training pipeline as BioMime, conditional generative models can be used to another field to capture a biomechanical system and predict muscle lengths from the kinematics of a musculoskeletal model.

We are motivated by the demand on tracking muscle length changes during a subject's movement from a limited number of joint angles. Muscle lengths are correlated with the kinematics of a subject and can only be fully defined when the whole set of joint angles are provided. However, the number of the joint angles that can be recorded during an experiment might be limited, for example due to the occlusion of the markers. It is not possible to directly regress muscle lengths from a limited set of joint angles. However, if we convert the regression problem to a generation problem and embed the unknown joint angles into some latent representations, we will still be able to predict the muscle lengths with expected limited joint angles by morphing the existing muscle length sets.

To give an example, assume that we want to track finger, hand, and forearm muscle lengths during hand and wrist movements. Only joint angles of the three wrist degrees-of-freedom (DoFs) can be measured while the other joints, such as the metacarpophalangeal (MCP) and proximal interphalangeal (PIP), are not recorded. If we want to track the muscle lengths during wrist flexion (the wrist angles are known) combined with hand pinch (MCP and PIP unknown), movement **A**, and we know the muscle lengths during another movement **B** where the hand also pinched, then this is a generation problem similar to what we have solved by BioMime in modeling the volume conductor system. What we need to do is to morph the existing muscle lengths during movement **B** to combine the wrist flexion movement. The wrist movement in movement **B** can be random, e.g., wrist extension, pronation, etc.

Problem Formulation

Tracking muscle lengths \mathbf{y} given a set of joint angles \mathbf{x} can be formulated as $\mathbf{y} = f(\mathbf{x})$. If \mathbf{y} is fully defined by \mathbf{x} , then this is a regression task. However, if \mathbf{x} cannot fully define \mathbf{y} as shown in the above example, the task is converted to a generation task with a new formulation $\mathbf{y} = f(\mathbf{x}, \mathbf{z})$, where \mathbf{z} is the unspecified angles. In the manuscript of BioMime, \mathbf{x} is the specified conditions \mathbf{c}_s (well-defined physiological parameters), and \mathbf{z} the unspecified conditions \mathbf{c}_u . Similar to BioMime, the unspecified conditions \mathbf{z} can be obtained by sampling from a prior or by implicitly decoding from an input muscle length sample \mathbf{y}_0 :

$$\mathbf{y} = \begin{cases} f(\mathbf{x}, \mathbf{z}), \mathbf{z} \in N(0, \mathbf{I}) \\ f(\mathbf{x}, \phi^{-1}(\mathbf{y}_0)) \end{cases} \quad (4)$$

The specified joint angles \mathbf{x} include joint angles of three wrist DoFs (flexion/extension, supination/pronation, radial/ulnar deviation). The unspecified conditions \mathbf{z} captures the other joint angles, e.g., angles at MCPs and PIPs, and the properties of the biomechanical system.

Dataset Preparation

We used OpenSim to export muscle lengths given the hand, wrist, and forearm movement of an open-source musculoskeletal (MSK) model (34). The MSK model is the same as in the

manuscript. A total of nine joint angles were used to drive the MSK model, including three wrist DoFs (flexion/extension, supinator/pronation, and radial/ulnar deviation) and the MCP and PIP joints of the first three fingers. The MCP and PIP of the fourth and fifth fingers were assigned the same value as the third finger. The angles were calculated from the motion capture data. Details can be found in (40). Lengths of 11 muscles were exported using OpenSim, including Extensor carpi radialis brevis (ECRB), Extensor carpi radialis longus (ECRL), Extensor carpi ulnaris (ECU), Extensor digitorum communis index (EDCI), Extensor digiti minimi (EDM), Extensor pollicis longus (EPL), Flexor Carpi Radialis (FCR), Flexor carpi ulnaris (FCU), Flexor digitorum profundus index (FDPI), Flexor digitorum superficialis index (FDSI), and Palmaris Longus (PL). These muscles are mostly used during hand, wrist, and forearm movement.

Data from eight subjects were used to prepare for the dataset. The subjects were required to do a sequence of hand and wrist movements and the motion capture data were recorded at the same time. Detailed protocols can be found in (40). During data preprocessing, we manually removed the trials in which at least one DoFs of joint angles were unreliable due to the occlusions of the markers. The joint angles were downsampled to 25 Hz and a random window of 4 seconds was cropped in each trial. In total, there are 24,400 samples in the dataset, each consisting of 9 joint angles and 11 muscle lengths. We augmented the dataset by simulating more movements with two strategies. First, one-DoF wrist movement was combined with one hand movement (e.g., input1: wrist flexion, input2: hand close, output: wrist flexion + hand close). Second, the hand movements in two 2-DoF hand and wrist movements were swapped (e.g., input1: wrist flexion + hand close1, input2: wrist pronation + hand close2; output1: wrist flexion + hand close2, wrist pronation + hand close1). Data augmentation increases the diversity of the samples in the existing dataset and provides the ground truth muscle lengths for validating the morphing performance of the model. Finally, there are 83,000 samples in the augmented dataset. We divided the dataset into the training dataset and the testing dataset by subjects to test the model's performance on generalizing among subjects. Two subjects were randomly chosen, and their data were used as the test dataset.

Model Architecture

The model has the same architecture as BioMime, an encoder-decoder structured generator and a discriminator. The encoder, decoder, and discriminator are composed of multi-layer perceptron (MLP). The encoder has two hidden layers each followed by an activation operation (ReLU). The input dimension is 11 (dimension of muscle lengths), hidden dimension 128, and output dimension 64. The output of the encoder is passed to two linear layers (output dimension 16), which estimate the mean and variance of the approximate posterior. During training, the approximate posterior is sampled by the reparameterization trick. During inference, the expectation of the posterior is used as the latent representation. The latent representation is then concatenated with the specified conditions (3 joint angles) before passed to the decoder. The decoder has three hidden layers each followed by a ReLU (input dimension 19, hidden dimension 128, output dimension 11). The discriminator has two hidden layers (input dimension 14, hidden dimension 32, output dimension 1), each followed by a ReLU.

Training Pipeline

The model is trained in the same way as BioMime. There are three losses in the objective function of the generator:

$$\mathcal{L}_G = \lambda_1 \mathcal{L}_{GAN} + \lambda_2 \mathcal{L}_{KL} + \lambda_3 \mathcal{L}_{cyclic} \quad (5)$$

where \mathcal{L}_{GAN} is an adversarial loss that evaluates whether the generated muscle length is realistic. \mathcal{L}_{KL} is the Kullback-Leibler divergence between the predicted distribution of the latent feature and the standard normal distribution. \mathcal{L}_{cyclic} is the cycle-consistency loss. The hyper-parameters λ_1 was set 10, λ_2 0.1, and λ_3 5.

The loss function of the discriminator is the same as in BioMime’s training:

$$\begin{aligned} \mathcal{L}_D = & -\mathbb{E}_x[\log D(\mathbf{x}, \mathbf{c}_s)] - \mathbb{E}_x[\log(1 - D(\mathbf{x}, \mathbf{c}_r))] * 0.5 \\ & - \mathbb{E}_x[\log(1 - D(G(\mathbf{x}, \mathbf{c}_s), \mathbf{c}_s))] * 0.5 \end{aligned} \quad (6)$$

where \mathbf{x} is the ground truth muscle length output by OpenSim, \mathbf{c}_s is the specified conditions (3 joint angles), and \mathbf{c}_r is a set of randomly generated specified conditions.

The ratio between the discriminator and the generator updates was 1:1. The discriminator and the generator were trained for 100 epochs with Adam optimizer and a cosine annealing learning rate from 1e-3 to 1e-5. The number of input data in each mini batch was 32. Training took 42 seconds for each epoch, thus 1.2 hours in total.

Results

The model accurately generates the muscle lengths given an expected wrist movement and an implicit hand movement. We evaluated the accuracy of the model when it is used to morph a set of existing muscle lengths to a new wrist movement. This is tested on the augmented dataset. For example, in the dataset augmented by swapping, muscle lengths under wrist movement2 + hand movement1 are the ground truth of the results by morphing wrist movement1 + hand movement1 to wrist movement2 + hand movement2. The nRMSE is 1.26% when evaluated on the augmented test dataset. A representative example of comparison between muscle lengths generated by the model and the ground truth is shown in Supplementary Fig. S6.

Different from the volume conductor system in the manuscript, the biomechanical system provides information about the human body components (e.g., muscles), movement, and forces. By showing that a conditional generative neural network similar to BioMime can predict reliable muscle lengths given a set of joint angles, we envision a broad use of BioMime in capturing different biophysical systems.

Supplementary Figures

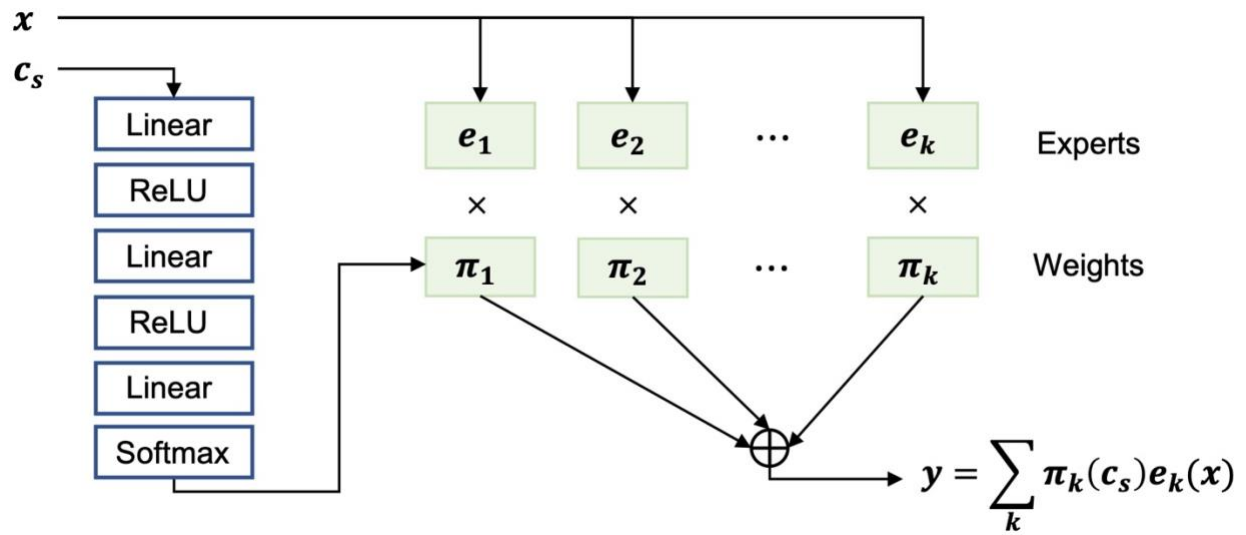


Fig. S1. Time-scaling module in decoder. The proposed time scaling module is a temporal pooling/unpooling bank with learned weights. The weights are conditioned on the desired specified conditions by a feedforward layer. This module is specialized for dilating or compressing signals in time domain.

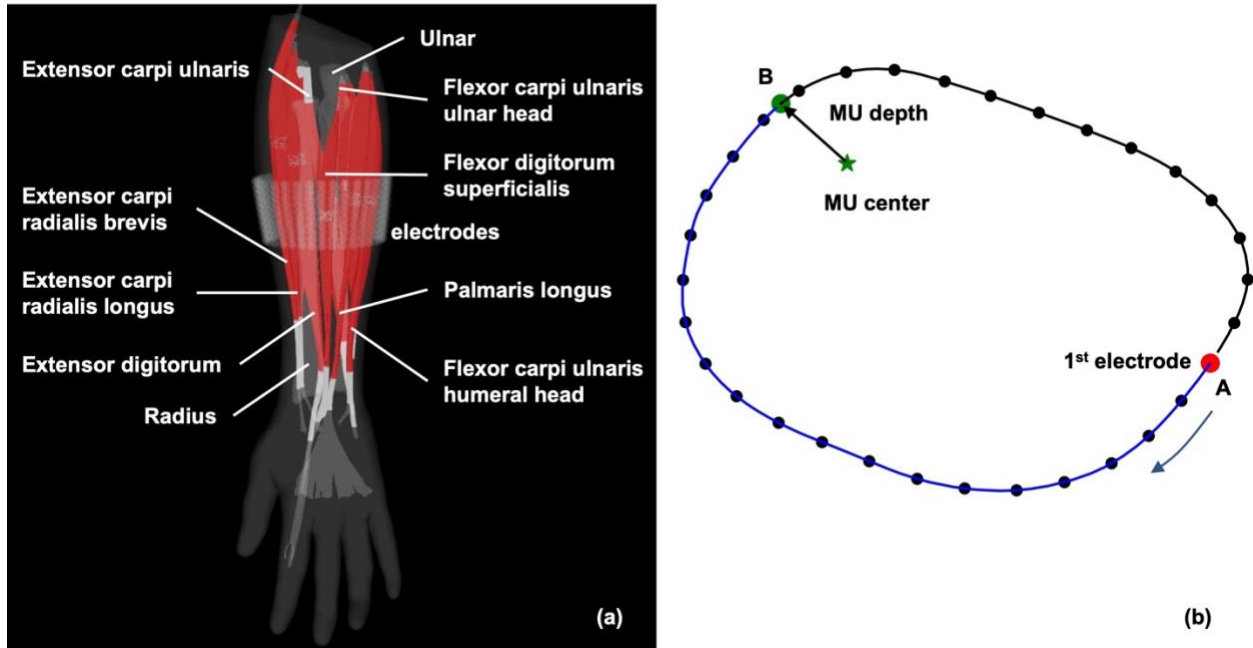


Fig. S2. Illustration of realistic numerical model. **a**, The eight superficial muscles are visualized in the realistic forearm model. The radius and ulnar are shown in grey volumes. Electrode grid with 10×32 channels covers the muscle belly of the most forearm muscles. **b**, Definitions of the depth and medial-lateral position of the MU center. MU center is defined as the centroid of all the intersection points between the fibers in this MU and the reference plane. The closest distance between the MU center and the skin surface is regarded as the depth of the MU. The medial-lateral position of the MU is represented by the radian of the MU center with respect to the reference electrode, \widehat{AB}/p , where p is the perimeter of the cross section.

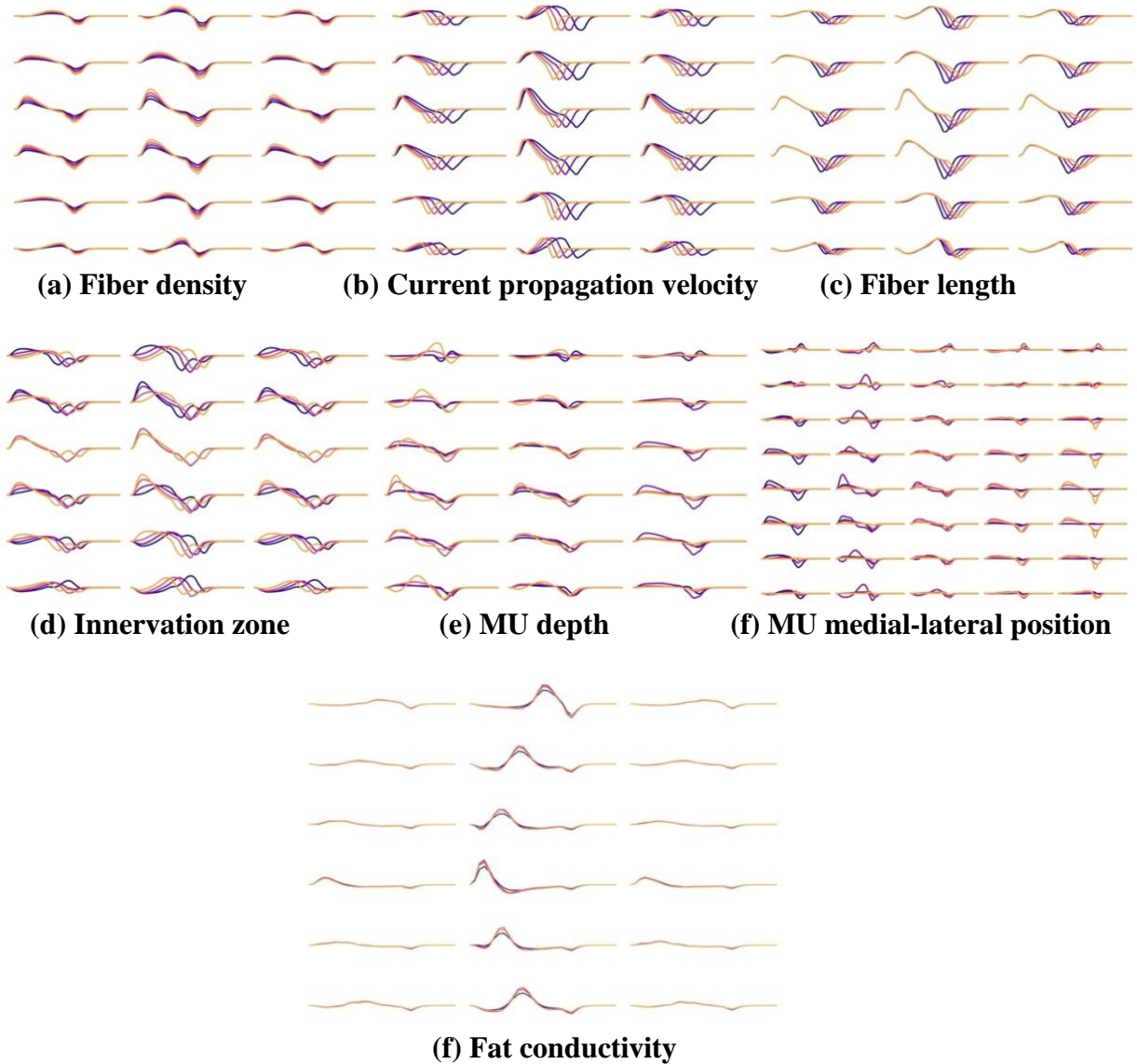


Fig. S3. Variations of spatial-temporal attributes of MUAP with changes of (a) fiber density, (b) current propagation velocity, (c) fiber length, (d) innervation zone, (e) depth of MU center, (f) medial-lateral position of MU center, and (g) fat conductivity. Color from deep to light denotes the variation of the normalized conditions from 0.5 to 1.0. Note, here, the MUAPs were generated by a numerical model with a cylindrical volume conductor to show clear variations of the MUAPs with the conditions. (a) Fiber density mainly changes the amplitude of the waveforms. (b) Current source propagation velocity scales the signal in the temporal domain (c) Fiber length primarily modifies the duration of the signal. (d) The impact of innervation zone is much more complex. It moves the peak of the signals in the longitudinal direction and modifies the non-propagating component of the waveform (41). (e) The depth of MU center changes the low-pass filtering effect, such that the amplitude and the spatial distribution are changed. (f) The medial-lateral position of MU mainly alters the spatial distribution of MUAP transversely. (g) The fat conductivity changes the amplitude of the waveforms.

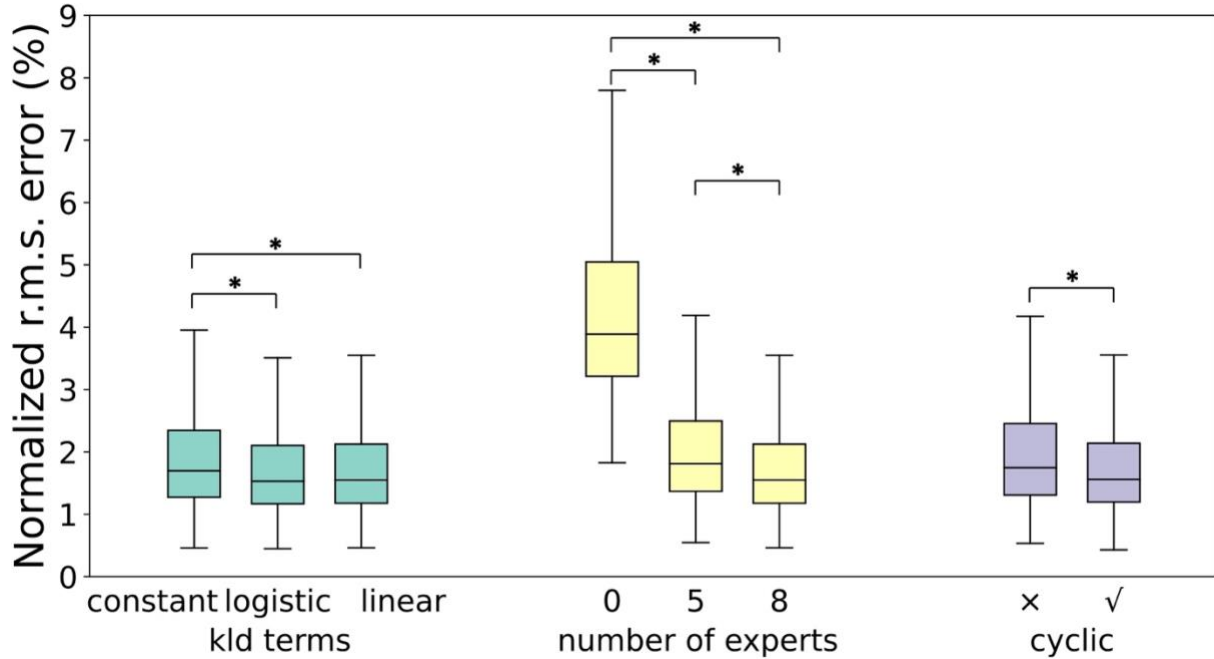


Fig. S4. Boxplot of accuracy when changing schedules of KL divergence terms, increasing the number of experts in the time-scaling module, and including cycle-consistency loss or not. The accuracy was measured in the normalized root mean square error between the generated MUAP signals and the ground truth signals and was evaluated for all realizations with independently generated samples. The one-way Welch’s ANOVA of the generation accuracy on the KL divergence terms revealed a statistically significant main effect ($p < 0.001$). Post hoc comparisons using the Games-Howell post hoc procedure indicated that applying logistic or linear annealing schedule significantly improved the generation accuracy and reduced the variance than using the constant schedule ($p < 0.001$). There was also a statistically significant difference between the means of accuracy with the number of experts (Welch’s one-way ANOVA, $p < 0.001$). The Games-Howell post hoc showed that the mean difference between the three levels all reached significance ($p < 0.001$). A Wilcoxon signed-rank test showed that including the cycle-consistency loss significantly improved the generation accuracy ($Z = -17.143$, $p < 0.001$). We also observed that with the cycle-consistency loss, the training was more stable.

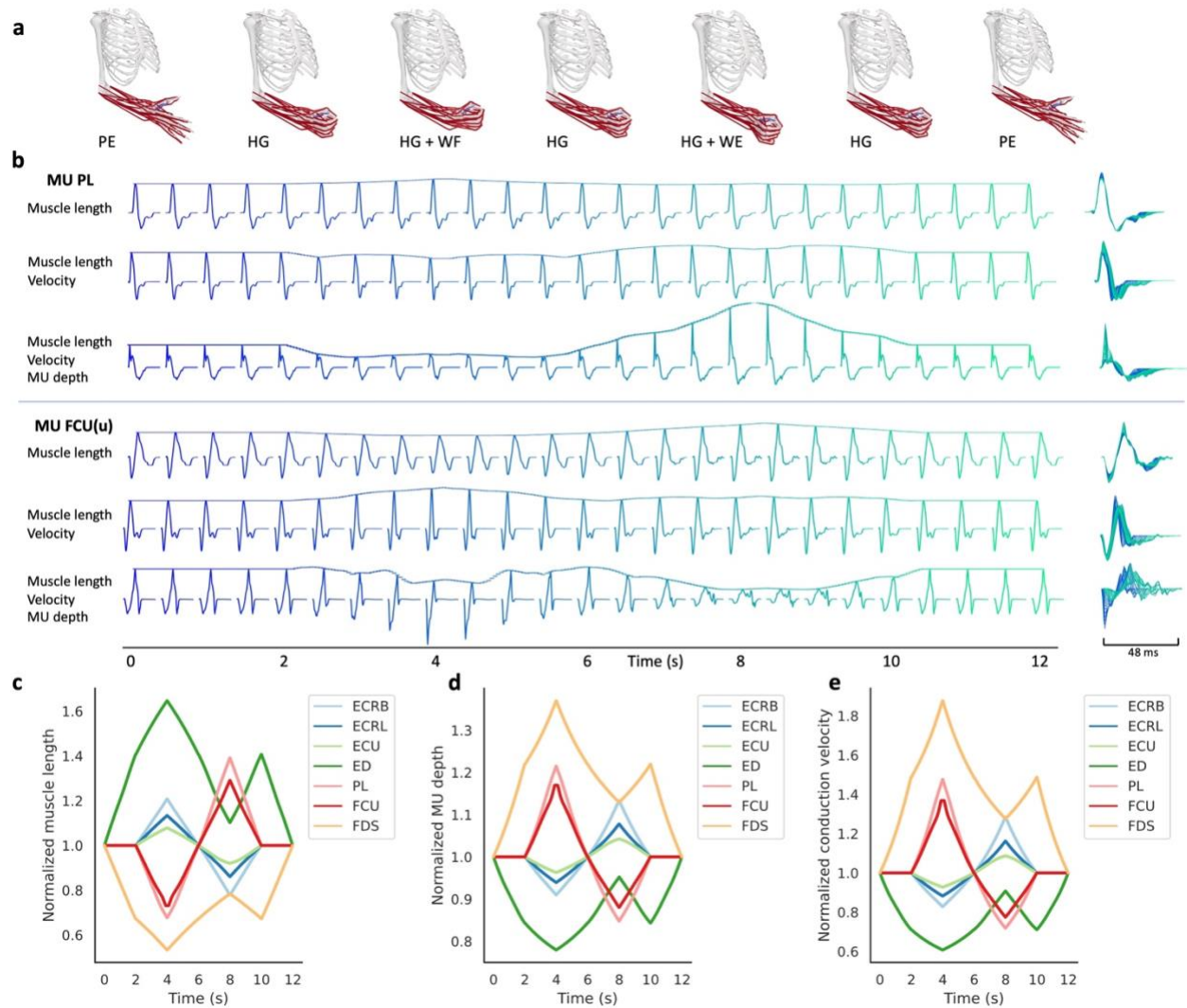


Fig. S5. BioMime predicts MUAP changes during a movement of a musculoskeletal model. **a**, Sequence of the movements. **b**, Two representative MUAPs generated by BioMime. The upper MUAP is from Palmaris longus, PL and the lower MUAP from the ulnar head of Flexor carpi ulnaris, FCU(u). In each of the three rows, MUAP in the first row are morphed using the muscle length profiles given by the MSK model using OpenSim. MUAPs in the second row are morphed with changes of muscle length and the current source propagation velocity. MUAPs in the third row are morphed with changes of three parameters, muscle length, velocity, and MU depth. **c**, Normalized muscle length profiles from the musculoskeletal model. **d**, Normalized MU depth. **e**, Normalized current source conduction velocity.

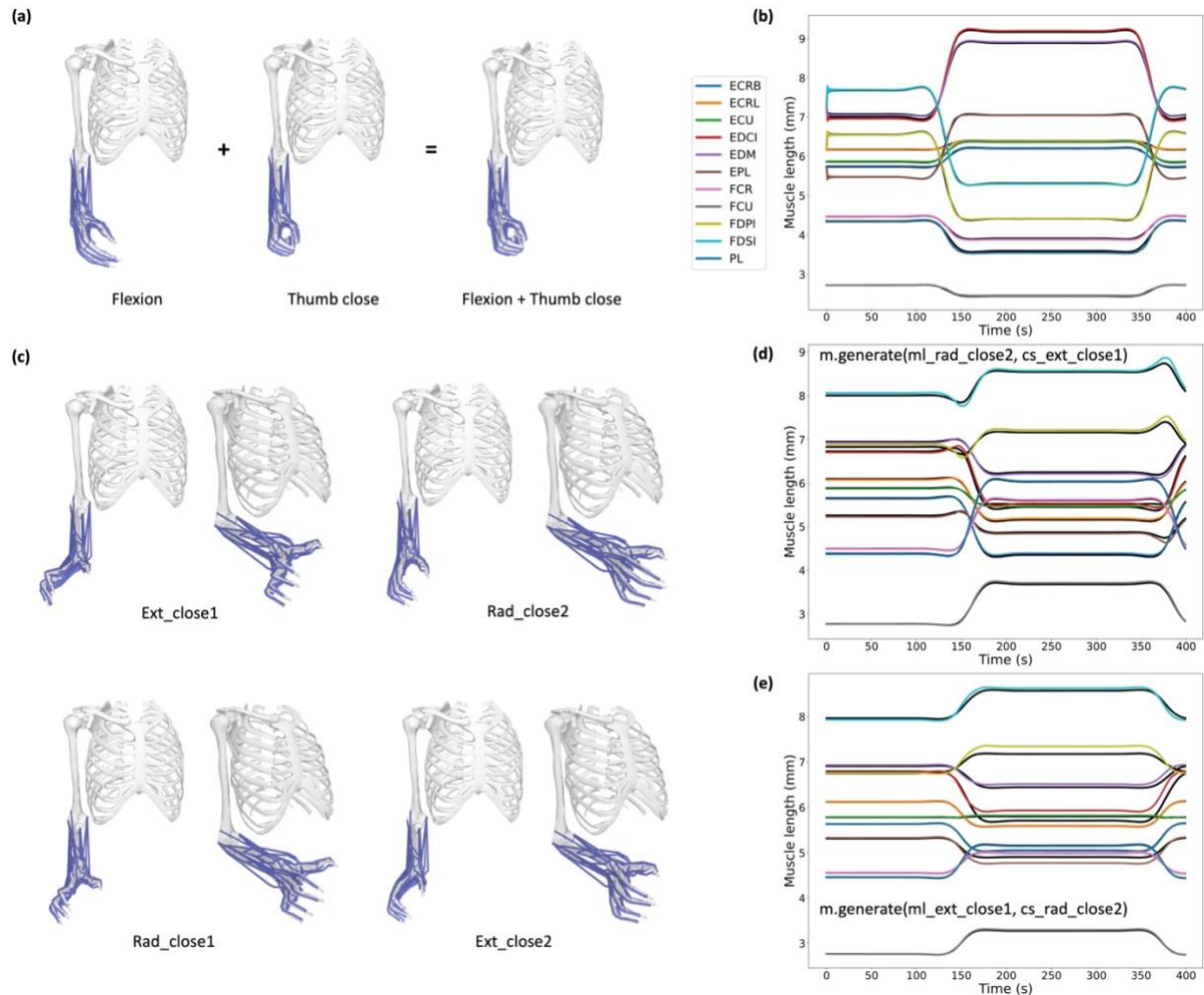


Fig. S6. Muscle lengths predicted by the generative model. **a**, A wrist flexion movement was combined with a thumb close movement. The combined movement was imported to OpenSim to export the ground truth muscle lengths. **b**, Muscle lengths predicted by the generative model when the two 1-DoF movements in **a** are combined. The normalized root mean square error (nrms) between the output of the model and the ground truth is 0.32%. **c**, The hand close movements in two 2-DoF movements (Extension and close1, Radial deviation and close2) are swapped, resulting in another two 2-DoF movements (Radial deviation and close1, Extension and close2). **d**, Muscle lengths predicted by the generative model by keeping the hand close2 in Rad_close2 while combining wrist extension in Ext_close1. nRMSE between the output of the model and the ground truth is 0.66%. *ml_rad_close2* is the input muscles lengths during Rad_close2 movement. *cs_ext_close1* is the wrist angles (the specified conditions) during Ext_close1 movement. **e**, Muscle lengths predicted by the generative model by keeping the hand close1 in Ext_close1 while combining wrist radial deviation in Rad_close2. nRMSE between the output of the model and the ground truth is 1.27%. *ml_ext_close1* is the input muscles lengths during Ext_close1 movement. *cs_ext_close1* is the wrist angles (the specified conditions) during Rad_close2 movement.

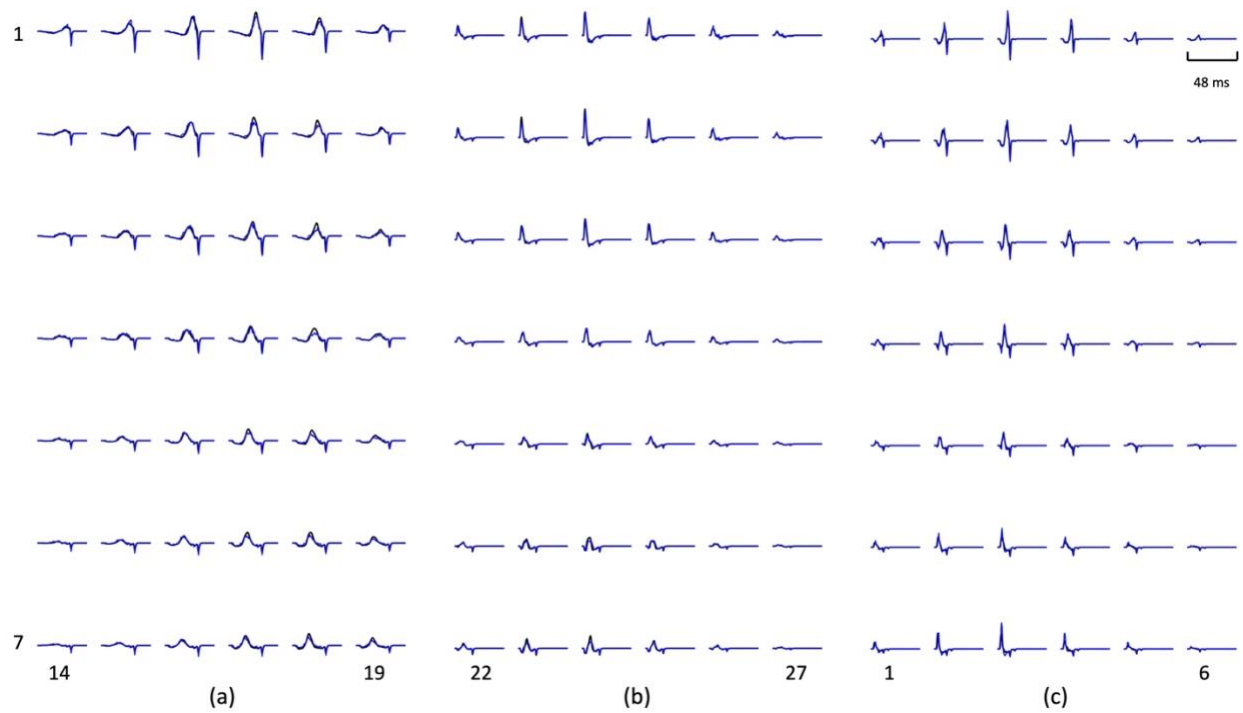


Fig. S7. Representative MUAPs simulated by the fine-tuned BioMime. MUAPs have been normalized to the maximum amplitude among all channels. The 32×10 electrode grid was cropped to display the channels that have obvious waveforms. The numbers besides the channels are the indices of the rows and columns of the selected channels. The simulated MUAPs are plotted in blue lines while the ground truth black. **a**, One MUAP from muscle Extensor carpi radialis longus with fat conductivity 0.0718 S/m. The nRMSE between the simulated MUAP and ground truth is 0.012. **b**, One MUAP from muscle Extensor carpi ulnaris with fat conductivity 0.215 S/m. The nRMSE between the simulated MUAP and ground truth is 0.009. **c**, One MUAP from muscle Palmaris longus with fat conductivity 0.024 S/m. The nRMSE between the simulated MUAP and ground truth is 0.010.

Supplementary Tables

Table S1. The network structure of encoder and discriminator in BioMime

Generator-Encoder			Discriminator		
Layer	Parameters	Output	Layer	Parameters	Output
Conv3d	3, 2, 1	[16, 48, 5, 16]	Conv3d	3, 1, 1	[16, 48, 5, 16]
Conv3d	3, 2, 1	[32, 24, 3, 8]	Conv3d	3, 2, 1	[32, 24, 3, 8]
Conv3d	3, 2, 1	[64, 12, 2, 4]	Conv3d	3, 2, 1	[64, 12, 2, 4]
Conv3d	3, (2, 1, 1), 1	[128, 6, 2, 4]	Conv3d	3, (2, 1, 1), 1	[128, 6, 2, 4]
Conv3d	3, 1, 1	[256, 6, 2, 4]	Conv3d	3, 1, 1	[256, 6, 2, 4]
Flatten		[256 * 6 * 2 * 4]	AvgPool3d	(6, 2, 4)	[256, 1, 1, 1]
Linear (μ)	12288 \rightarrow 16	[16]	Conv3d	1, 1, 0	[1, 1, 1, 1]
Linear (σ)	12288 \rightarrow 16	[16]	Squeeze		[1]

* Each Conv3d in the encoder is followed by a PReLU layer. Each Conv3d in the discriminator is followed by a LeakyReLU with negative slope equal to 0.03.

Table S2. Informativeness score (%) of indicating specified conditions c_s from the latent features z .

Hidden layers	c_{s_1}	c_{s_2}	c_{s_3}	c_{s_4}	c_{s_5}	c_{s_6}
2 layers	50.85	37.87	37.89	32.99	24.10	14.06
3 layers	50.43	31.98	53.59	30.71	19.47	11.58
4 layers	49.75	36.17	53.18	29.89	23.54	11.36
5 layers	48.09	34.01	51.51	34.02	26.23	13.57
6 layers	16.13	16.13	19.10	13.6	5.00	7.50

¹ The six specified conditions from c_{s_1} to c_{s_6} are number of muscle fibers, depth of MU center, medial-lateral position of MU center, position of innervation zone, current propagation velocity, and fiber length, respectively.

² Non-linear regressors with two to six hidden layers (hidden dimension 256) were trained.

³ One possible reason that the informativeness score suddenly decreased when the number of hidden layers in the regressor reached six is that the model overfitted the training dataset.

Table S3. Comparison of Runtimes for the Numerical Model¹ versus BioMime

Numerical Model	General forward solution	Fiber basis points	MUAP simulation
Time	13 s/electrode	120 s	30.8 s
BioMime	Preparation for the two datasets ²	Training and fine-tuning	MUAP simulation
Time	19.7 + 98.7 hours	120 + 54 hours	0.287 s

¹ Time for the numerical model is from (21).

² The first dataset is the dataset that we described in the original manuscript. The first dataset has six specified conditions and is used to train the base BioMime. The second dataset includes one more specified condition (fat conductivity). We fine-tuned the base BioMime on the second dataset.

Supplementary Algorithms

Algorithm S1: Training procedure of BioMime

Input: MUAP samples labelled with their specified conditions $\{x_0, c_0\}$, the desired conditions c_s , randomly sampled conditions c_r , number of training epochs S , hyperparameters $\lambda_1 = 10.0$ for \mathcal{L}_{GAN} , *anneal_func* for linearly increasing the weight λ_2 of \mathcal{L}_{KL} , $\lambda_3 = 0.5$ for \mathcal{L}_{cyclic}

$\theta_G, \theta_D \leftarrow$ initialize network parameters

for $n = 1$ to S **do**

$\rho_r \leftarrow D(x_0, c_0)$

real sample + real condition

$\rho_{f1} \leftarrow D(G(x_0, c_s), c_s)$

fake sample + real condition

$\rho_{f2} \leftarrow D(x_0, c_r)$

real sample + random condition

$\mathcal{L}_D \leftarrow 0.1 * ((1 - \rho_r)^2 + (\rho_{f1}^2 + \rho_{f2}^2) / 2)$

$\theta_D \leftarrow \theta_D - \alpha \nabla_{\theta_D} \mathcal{L}_D$

update discriminator

$\tilde{x}, \mu, \log(\sigma^2) \leftarrow G(x_0, c_s)$

generate by morphing

$\hat{x} \leftarrow G(\tilde{x}, c_0)$

reverse generation

$\rho \leftarrow D(\tilde{x}, c_s)$

$\mathcal{L}_{GAN} \leftarrow (1 - \rho)^2$

$\mathcal{L}_{cyclic} \leftarrow \|x_s - \hat{x}\|_2^2$

$\mathcal{L}_{KL} \leftarrow -(1 + \log(\sigma^2) - \mu^2 - \sigma^2) / 2$

$\lambda_2 \leftarrow$ *anneal_func*(n)

$\mathcal{L}_G \leftarrow \lambda_1 \mathcal{L}_{GAN} + \lambda_2 \mathcal{L}_{KL} + \lambda_3 \mathcal{L}_{cyclic}$

$\theta_G \leftarrow \theta_G - \alpha \nabla_{\theta_G} \mathcal{L}_G$

update generator

end for

Algorithm S2: Generating by morphing

Input: Desired specified condition c_s and input sample x

Output: Simulated MUAPs conditioned on the desired system states \tilde{x}

```
 $\mu, \sigma \leftarrow \text{Encoder}(x)$   
 $z \leftarrow \mu$   
 $\tilde{x} \leftarrow \text{Decoder}(z, c_s)$   
Return  $\tilde{x}$ 
```


Algorithm S3: Generating by sampling

Input: Desired specified condition c_s

Output: Simulated MUAPs conditioned on the desired system states \tilde{x}

$\mathbf{z} \sim N(\mathbf{0}, \mathbf{I})$

$\tilde{x} \leftarrow \text{Decoder}(\mathbf{z}, c_s)$

Return \tilde{x}